# COMBINATORIAL TECHNIQUE FOR BIOMATERIAL DESIGN

A Thesis
Presented to
The Academic Faculty

by

Gracy A. Wingkono

In Partial Fulfillment
of the Requirements for the Degree
Master of Science in the
School of Chemical and Biomolecular Engineering

Georgia Institute of Technology
July 2004

COMBINATORIAL TECHNIQUE FOR
BIOMATERIAL DESIGN

Approved by:

Dr. Carson Meredith, Chair

Dr. Mark Prausnitz

Dr. Joseph Schork

Date Approved: July 1, 2004

*For everyone who has touched my life*

*and helped me to keep learning along the way.*

## ACKNOWLEDGEMENTS

I would like to express my heartfelt thanks to God. He has been giving me the direction, support, endurance, courage, and patience in the course of my study.

My special thanks to Dr. Carson Meredith for his continuous guidance, patience, and support. I am very grateful to him for giving an endless inspiration throughout my whole time being his graduate student.

I would like to gratefully acknowledge Dr. Andres Garcia, Dr. Christopher Jones and Dr. Clifford Henderson along with their research groups for their help with Fluorescence Microscopy, FTIR and Ellipsometry. I would like to thank Dr. Mark Prausnitz and Dr. Joseph Schork as well, for dedicating their valuable time to serve on my committee.

The Advanced Polymer Thin Films and Colloid Materials research group is an amazing group; I always enjoy the great experience of being a part of the group and working with such talented individuals. I want to thank all group members for creating such a wonderful atmosphere for research. Special thanks to Krishna Marla, Santanu Chattopadhyay, and Joe Sormana, who have been role models and mentors to me.

In particular, I wish to thank my Mom and Dad, Mami, Meity, and also my dear friends Robert C. McManis, Yeny Hudiono, Bernard Loo, Aang Daniel, Manish Gupta, Preeti Chandra, and Ashwini Sinha who have been the vessel of blessings through whom God has been working in my life. A lot of things happened during my study toward the completion to my Master degree; their continuous support and sincere care had strengthened me through them all.

## TABLE OF CONTENTS

## LIST OF TABLES

## LIST OF FIGURES

## GLOSSARY OF SYMBOLS AND ABBREVIATIONS

| | | |
|---|---|---|
| **φ** | Weight fraction | g/g |
| ECM | Extra-cellular Matrix | |
| h | Film thickness | μm |
| MDI | 4,4 Methylene bis-phenyl diisocyanate | |
| PCL | Poly(ε-caprolactone) | |
| PEG | Poly(ethylene glycol) | |
| PEGPU | Poly(ethylene glycol) crosslinked with Poly(urethane) bonds | |
| PETA | Penta Erythritol Triacrylate | |
| PS | Poly(styrene) | |
| Ra | Roughness | nm |
| Si | Silicon | |
| T | Annealing temperature | $^{o}$C |
| Tg | Glass transition temperature | $^{o}$C |
| Tm | Melting point | $^{o}$C |
| TQ | Quenching temperature | $^{o}$C |
| VASE | Variable Angle Spectroscopic Ellipsometer | |
| x | Coating Distance measured from the initial blade position | mm |
| y | Paint Distance | mm |

## SUMMARY

Combinatorial techniques have changed the paradigm of materials research by allowing a faster data acquisition in complex problems with multidimensional parameter space. The focus of this thesis is to demonstrate biomaterials design and characterization via preparation of two dimensional combinatorial libraries with chemically-distinct structured patterns. These are prepared from blends of biodegradable polymers using thickness and temperature gradient techniques.

The desired pattern in the library is chemically-distinct cell adhesive versus non-adhesive micro domains that improve library performance compared to previous implementations that had modest chemical differences. Improving adhesive contrast should minimize the competing effects of chemistry versus physical structure. To accomplish this, a method of blending and crosslinking cell adhesive *poly(ε-caprolactone) (PCL)* with cell non-adhesive *poly(ethylene glycol) (PEG)* was developed. We examine the interaction between MC3T3-E1 osteoblast cells and PCL-PEG libraries of thousands of distinct chemistries, microstructures, and roughnesses.

These results show that cells grown on such patterned biomaterial are sensitive to the physical distribution and phases of the PCL and PEG domains.

We conclude that the cells adhered and spread on PCL regions mixed with PEG-crosslinked non-crystalline phases. Tentatively, we attribute this behavior to enhanced physical, as well as chemical, contrast between crystalline PCL and non-crystalline PEG.

# CHAPTER 1

# INTRODUCTION

## 1.1. Background

The application of biodegradable materials in the medical field initially started with the introduction of resorbable sutures. Now this field has grown to encompass tissue engineering and other therapies. Tissue engineering itself has evolved from designing simple "biocompatible" scaffolds towards developing "bioactive" materials for controlling cellular and physiologic responses [1-8].

Bioactive polymers could be used in tissue engineering scaffolds that support and regulate key elements in cellular responses such as adhesion, growth and function of target cells. Studies have shown that both chemical and physical surface properties control those cellular response [3, 4, 9-16]. Hence, superior biomaterial design requires a thorough understanding of signaling chemistry as well as of physical and non-specific chemical surface features and their effects on cellular responses.

Many studies focused on the surface chemical aspects of signaling. Various ways of modifying surface adhesiveness such as using different polymer or coating/grafting with certain functional groups on the surface have been explored. For example, a certain amino acid sequence RGD is well-known to be recognized by integrins and often necessary for cell adhesion. RGD is one of known cell-adhesive domain of Fibronectin. Most of cell lines for subsequent adhesion [11, 12, 17-22]. In addition, extracellular

matrix proteins such as collagen and fibronectin are specifically important for adhesion on the surface in fibroblastic cells [1-3, 9, 11, 12].

The importance of physical surface features in biomaterial design is tremendous. Micro patterning of living mammalian cells has made significant contributions to fundamental cellular biology, tissue engineering, and cell-based bioelectronics since spatial control of cellular adhesion and growth is critically important in these fields [4, 5, 9, 23]. It has been reported that cellular shape and movement (traction and migration) respond to the substrate mechanical strength of the biomaterial structure. This is crucial in several cases such as wound healing [24, 25].

It is already known that surface roughness, geometric spacing of adhesive and non-adhesive area, and surface mechanical properties can influence some cellular responses upon adhesion [1, 5, 9, 15, 26-32]. Cell behavior and cell fate dependence on cellular shape and anchorage in fibroblast cells have been studied for more than two decades [4, 5, 9, 15, 23, 33-35]. Integrin-mediated adhesion to **extra cellular matrix (ECM)** and cell shape *per se* have been shown to govern the life and the death of these cell lines [9, 35]. The ratio of adhesive to non- adhesive area, their spacing, and dimensions have been shown to be geometric controls of cellular life and death [9]. Much of this research has been done with surface patterning techniques adopted from microelectronics used to create surface with well-controlled properties [4, 11, 12, 23, 34].

But physical microstructure and topography of biomaterials have not been explored nearly as much as their mechanical and chemical properties, despite their importance. Metals and various industrial plastics that are widely used for medical implants, lack the molecular sequence and patterns crucial for normal cell function and therefore often

trigger aberrant cell responses in long term implantation [7]. Therefore more research linking chemical and physical surface properties with cell response are critical for future medical applications.

Major challenges in this scientific quest are limited time and scarcity of resources. Both stages in data acquisition - scanning through the vast combinations of parameters to create surfaces with different characteristics, and growing cells on each of those surfaces by observing its interaction with the surface - are the main limitations. Combinatorial and high-throughput techniques are two methods that provide answers to this challenge. Apart from providing an effective data acquisition, the large amount of data generated from combinatorial and high-throughput techniques requires equally effective and cost-efficient methods for analysis and evaluation. Data mining and data processing techniques are needed to cope with the large amount of information generated by these techniques [36].

Combinatorial techniques have only recently been applied successfully to both chemical and physical aspects of biomaterial design. Chemical synthesis of biodegradable polymers from a diverse set of different monomers has been shown to be successful [2, 3, 37-41]. Briefly, structurally different polymers from combinatorial library of tyrosine-derived polyarylates were synthesized in an array of small 20-ml glass vials. Each vial was charged with the appropriate mixture of monomers and reagents. The monomers were 8 different diacids and 14 different tyrosine-based diphenols. Chemical structure in diacids was used to create structural variations in the polymer backbone, while chemical structure of the diphenols was used to create structural variations at the

polymer pendant chain. From a library of systematically 112 polyarylates, correlations between structure-property-cellular interaction were demonstrated.

For the physical part, combinatorial methods have shown that phase separation of polymer blends can be utilized to create libraries of physical surface properties [1, 42]. Briefly, libraries of biomaterial properties were created combinatorially from composition and annealing temperature gradients. The gradients created diverse arrays of surface properties. It was successfully demonstrated that osteoblast cells cultured directly on those combinatorial surfaces showed different cellular response upon cell-biomaterial interaction. A similar approach is to be followed in this research.

Osteoblast is chosen as the mammalian cell lines used for cellular sample for this research. The reasons behind this choice are two-fold. From cellular biology, a lot of research has been done on this cell line, so the cellular characterization is well-established. From the future application of the novel biomaterial, osteoblast is known as one of the 'difficult-to-grow' cell line. One of the biggest interests in tissue engineering field is to learn how osteoblast can actually be regulated so that they can proliferate and function with certain desired performance by modulating the biomaterial properties.

## 1.2. Combinatorial Design of Biomaterial

### 1.2.1. Desired Properties of Biomaterial

An ideally engineered tissue comprising of live cells seeded into a synthetic degradable matrix would have the same mechanical properties as of the natural tissue it is designed to replace. The focus of this research is on osteoblast cells whose natural environment is a multi component ECM. Therefore, the desired biomaterial should

resemble ECM in its chemical, mechanical and surface properties. The polymer is chosen taking into account several factors as follows:

a. biocompatibility and degradability
b. ability to be patterned
c. contrast of adhesive and non-adhesive chemistry for cellular adhesion
d. mechanical strength.

The primary surface properties of interest in this research are chemical pattern, microstructure and surface roughness of different domains. Chemical pattern is created by using adhesive and non-adhesive polymer upon cellular attachment. Microstructure is the two dimensional pattern (size and spacing) of adhesive and non-adhesive sub domains. Surface roughness is the three dimensional topographic pattern of the surface and is dependent on microstructure. These will be used to describe surface properties of biomaterial that are related to cellular response.

### 1.2.2. Choice of materials

Previously, studies with **poly(d,l-lactide) (PDLA)** and **poly(caprolactone) (PCL)** system have been reported [1, 42]. These two biodegradable, biocompatible mates have a modest difference in hydrophobicity, which leads to some degree of preferential protein andsorption and cell attachment on PDLA. To explore a better hydrophobic versus hydrophilic contrast of the two polymers in the blend, we desire to develop a method for blending and patterning PEG and PCL.

Some properties of these polymers are given in Table 1.

Table 1. Physical Properties of the Pure Polymer (data was provided from supplier unless indicated otherwise).

| Polymer | Tg ($^{o}$C) | Tm ($^{o}$C) | Density (g/ml) | Water contact angle ($^{o}$) | Young's modulus (GPa) | Tensile strength (MPa) |
|---|---|---|---|---|---|---|
| PEG $M_w$ =2,000 | -44 | 49.1 | 1.104 | 20-25[43][1] | 3.68[43][2] | 2.55[43][3] |
| PCL $M_w$ =80,000 | -60 | 60 | 1.145 | 79.2 | 0.15 [42] | 20.1 [42] |

Young's modulus is the indicator how stiffness, or the amount of force required to elongate, i.e. the material elasticity. Tensile strength indicates the stress (force/area) at which a material can withstand breaking. From the values above, PEG is more flexible than PCL; but it has less material strength compared to PCL. Therefore, PEG and PCL mixtures may be suitable candidates for biomaterials with adjustable mechanical properties.

Both PEG and PCl are biocompatible and biodegradable. PEG is a well-known protein and cell-repellant surface. Increased PEG content in biomaterial has been proven to reduce protein adsorption and cell attachment [6, 38, 39, 44]. Many ECM and serum proteins have been shown to adsorb well on PCL, due to its hydrophobic character, which can potentially enhance cellular attachment on biomaterial surfaces [45, 46].

The drawback of using PEG is that especially at low molecular weight it is highly soluble in aqueous media [47]. Therefore, PEG needs to be crosslinked to slow down the dissolution to a time scale suitable for tissue engineering.

[1] Extrapolated value for PEG 2000.
[2] Extrapolated value for PEG 2000, as a function of porosity. Porosity ranges from 5 to 22%
[3] Extrapolated value for PEG 2000.

### 1.2.3. Choice of methods to design biomaterial

#### 1.2.3.1. Creation of patterning and contrast by phase separation

We desire a micropatterning method that can be extended to 3D tissue engineering scaffold. Previous studies have used phase separation of polymer blends induced by heating the film at temperatures within two-phase region [1]. This process is compatible with 2D and 2D scaffold and creates physically distinct sub domains on the surface of the polymer. We aim to use polymers with contrast in cell "adhesiveness", which phase separate to induce microstructure patterns of adhesive and non-adhesive sub domains.

Incompatibility in the chemical structure and molecular weight of the two components leads to phase separation. The use of blends with a library of surface properties resulting from phase separation can be generated within one combinatorial sample. Lower Critical Solution Temperature (LCST) or Upper Solution Temperature (UCST) phase separation induce different surface microstructure for the library as it has been studied previously [1, 42, 48] It is known that PDLA and PCL have an LCST. Here we expect that PEG-PCL with even greater difference chemistry, to phase separate also.

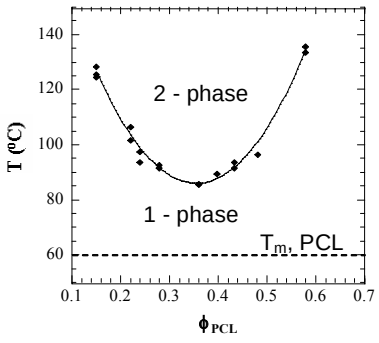


Figure 1. Cloud point curve showing LCST type phase separation in PDLA/PCL system [42].

There are two degrees of freedom that determine the state of a binary system with two phases. In this study, blend composition and annealing temperature are the variables chosen to control phase separation. Each **composition (φ)** and **annealing temperature (T)** will give different degrees of equilibrium phase separation. Elevated temperature for annealing basically moves the condition from 1 phase into 2 phase region (Figure 1). Generally, structures become larger as T moves deeper into 2-phase region and as time proceeds.

The high-throughput creation of surfaces with different characteristics is achieved by phase separation of the polymer blends. Therefore, φ, and T become possible control variables to determine the surface characteristics.

1.2.3.2. Creation of patterning and contrast by dewetting

Dewetting is another phenomenon in polymers, in which one polymer in liquid state forms droplets on another surface. Dewetting happens when wetting free energy becomes positive and film breaks into holes and droplets. One example of this is when polymers have significantly different surface energy. **Contact angle (γ)** can be used as an indicator for the balance of the opposing forces that led to film wetting or dewetting. Young's equation can be used to calculate relative surface tension of liquid film and solid substrate. Key variables controlling dewetting are the **film thickness (h)** and T.

Young's Equation:

$$\sigma_{sg} = \sigma_{sl} + \sigma_{lg} \cos \gamma \qquad (1)$$

where

$\sigma_{sg}$= solid-gas surface force/length

$\sigma_{lg}$= liquid-gas surface force/length[4]

$\sigma_{sl}$= solid-liquid surface force/length[5].

1.2.3.3. Creation of contrast by crystallization

Crystallization is important in that it creates surface roughness library and alters the presentation of chemical groups at the surface. Chain ordering in the crystallization process is dictated mainly by the structure of polymers. Solid and liquid-state multiphase polymer blends provide challenging research problems because the polymers' thermodynamic compatibility and relaxation rates dominate morphology[49]. During the annealing process, the supply of energy to the polymeric chains should at least cover the required energy for chain relaxation. This occurs when the temperature is higher than the **glass transition temperature (Tg),** and if the polymer crystallizes, the **melting point (Tm).**

Quenching below the Tm at the end of the annealing process is crucial for "freezing" the phase separated patterns at a desired point in evolution. Quenching is used also to control the crystallization rate in PCL or PEG.

The focus for crystallization in this research is limited only to its supramolecular level. In its supramolecular level forms, such as PEG-rich spherulitic forms, crystalline spherulites are constructed of ordered polymeric chains in lamellar structures. There are two competing rate processes: nucleation and growth.

We can control the ratio of nucleation and growth by varying the degree of undercooling in quenching[6]. Crystallization process is known to create different surface

[4] The larger $\sigma_{lg}$ value is, the stronger is the cohesive force.
[5] The smaller $\sigma_{sl}$ value is, the weaker is the adhesive force.

roughness in the sub domains [50]. This means we can use the **Quench Temperature (TQ)** to optimize surface roughness and crystallinity contrast between two sub domains. When TQ is extremely low, nucleation is faster than growth, a smaller structure and larger number of spherulites are expected in the result. Small amounts of undercooling favor rapid growth of existing nuclei.

For future reference, the interaction between crystallization and phase separation and the mechanism behind different crystallizability in the binary blend is still open for further research. The interaction between these two process affects the subsequent phase separation, and it is still not well understood. This is especially true for the cases when both polymers in binary blend are crystallizable [51]. Our aim is not to resolve this mechanism, but to use the phenomenon to generate diversity in surface features.

In brief, sub domains' surface roughness library created by crystallinity contrast is expected to be sensed and responded by adhering osteoblast. Hence, this research will also examine whether cellular response is also be related to the level of surface roughness contrast in the two sub domains.

### 1.2.4. Utilizing phase separation, dewetting, and crystallization in Combinatorial Technique for Biomaterial Design

Phase separation, dewetting and crystallization rate are shown to be good means for creating microstructure and surface roughness libraries by combinatorial method. This resembles the composition and gradients-generated library. The control variables are φ,

---

[6] Undercooling is defined as the difference between **quenching temperature (TQ)** and **melting point (Tm).**

T, h and TQ. For each sample, two variables from φ, T, and h can be used. This will create two dimensional arrays of data in the surface properties library. TQ will be varied for the whole library from each sample to find the optimum contrast desired. Once the optimum TQ is found, this value will be used through out the whole research study for all combinatorial samples in the library.

For imaging, crystallinity difference is used to observe the microstructure in an easier way. This is made possible because crystallinity contrast of the two phases can be observed by cross-polarized optical microscopy; the brighter area is the more crystalline phase of the two phases in the phase separated sample. PCL has a unique combination of properties to serve this purpose. Other than its crystalline nature, PCL is also the more hydrophobic part of the blend. Therefore, in PCL-PEG blends, brighter areas under a cross polarized microscope will correspond to the adhesive sub domain.

### 1.3. Significance

Potential applications of this research include cellular biology, tissue engineering, and material science. Fast, cheap and effective surface library design and scanning of properties and cellular response in combinatorial method can be used for biomaterial design for drug-delivery coatings, for example material whose porosity increases as the immersion time in aqueous media is increased; or for characterization and scanning of cellular response to different surface properties in cellular biology studies.

When translated into 3D structure, the significance of bioactive material could reach as far as tissue engineering for ‘difficult-to-grow’ cell lines, such as osteoblast. With proper design to adjust degradation time, 3D scaffold of bioactive material can enhance

invasion of osteoblast to re-grow its structure and gain appropriate strength; the scaffold degrade completely when the osteoblast structure is self-sufficient.

## 1.4. Experimental Method and Data Analysis for Combinatorial Scanning and Design

### 1.4.1. Polymer solution preparation

Poly(ethylene glycol) (**PEG**, $M_w$=2,000, Sigma-Aldrich), poly(ethylene oxide) (**PEO**, $M_w$=100,000, Sigma-Aldrich), poly(caprolactone) (**PCL** $M_w$=80,000, $M_w$/ $M_n$=1.43, Aldrich) were used for the polymer blend. Two methods to crosslink PEG were explored:

1. Chemical crosslink using **penta erithrytol triacrylate** (**PETA**, Sigma-Aldrich) as crosslinker and activated by UV
2. Chemical-physical crosslink using **4,4 Methylene bis-phenyl diisocyanate** (**MDI,** Sigma-Aldrich) and thermally activated.

UV-activated crosslink was created by incorporating PETA into PEG at concentration of 10% which is based on the correlation to Gel Fraction determined in the previous study [52].

Another method to get PEG crosslinked was by using thermal-activated MDI to produce a **PEG-polyurethane (PEGPU)**. MDI was prepared in chloroform, then mixed into PEG at stoichiometric amount (each at 30% weight solution in chloroform before being mixed) and after that the mixture is heated at 90$^o$ C under 600 rpm stirring for 6 minutes. Then more MDI was added up to 30% excess to the solution and the mixture was continuously stirred for another 2 minutes. Finally, chloroform was added to make 5% weight solution.

In order to get a better contrast of the phase separation in our research, the crystallization rate difference between crosslinked PEG and PCL was magnified by quenching the freshly coated film in an ice bath rather than quenching it to the room temperature.

### 1.4.2. Silicon surface preparation

Silicon wafers were obtained from commercial suppliers. **Silicon (Si)** wafers provided by Silicon Inc., resistivity 1-10 Ohms-cm were used as the substrate where the polymer blend film is coated on. Silicon surface was precleaned to remove the oxide layer. This ensured improved film attachment on the surface during contact with water in cell culture step. Etching steps were described in details elsewhere. In brief, chips were first immersed in piranha solution (30% hydrogen peroxide/70% sulfuric acid) for an hour, then etched with **Buffered Oxide Etchant (BOE) 1:6** provided by VWR for 25 minutes, followed by immersion in $NH_4F$ for 5 minutes and finally air dried.

### 1.4.3. Film coating and thermal treatment

A composition gradient film library was prepared using a combinatorial technique described in detail elsewhere [13]. In brief, a PCL solution in chloroform was pumped into a mixing vial (initially filled with PEO-PETA solution) while the mixture was withdrawn. A third automated syringe extracted the φ gradient from the vial and deposited it as a thin stripe on a Si chip (24x24 mm). The distance measured from initial first drop of liquid on the silicon within the stripe is termed **paint distance (x).** The paint distance corresponds to φ gradient. A knife-edge coater was used to spread the liquid stripe as a film at orthogonal direction to the φ gradient. The distance measured from the

initial edge where coating starts is termed **coating distance (y).** Annealing over T-gradient from $40^{o}$ C to $70^{o}$ C for 2 hours was achieved by using a T-gradient heating stage positioned orthogonal to the φ gradient. Phase-separated structure from a binary blend film was achieved by annealing process [42]. Phase separation process was proven to be completed by 2 h of annealing [1]. Annealing was followed by quenching to the room temperature. For UV-initiated crosslinking[7], curing under a UV Lamp (Oriel Instruments) was done at room temperature for 40 minutes (475 W, 248 nm filter, intensity=1.4 to 1.5 mJ/s.cm$^2$) after annealing and quenching.

Thickness gradient in y direction was created by using different coating speed. Thermal gradient is orthogonal to y direction. Annealing was performed over T-gradient from $80^{o}$ C to $110^{o}$ C for 2 hours. The follow up treatments were similar to composition gradient films.

### 1.4.4. Surface Characterization

Microstructures at various positions in the libraries were characterized with an automated Optical Microscope (with cross-polarized configuration, or phase contrast). Image analysis was performed with Image-Pro Plus Version 4.5.1.22 Media Cybernetics, Inc., an image processing tool. Surface roughness and topography were captured with AFM (SPM Explorer, Thermomicroscope).

The formation of gradients in composition was confirmed using a Fourier Transformed Infrared Spectrophotometer (Bruker). Spectral analysis was done with PEAKFIT software. Thickness was measured with WVASE Ellipsometer (J.A. Woolam).

[7] For PETA-PEO system only

The standard deviation for FTIR data ranged from 0.14 to 24.2% relative to the mean value.

#### 1.4.5. Scanning of cellular-biomaterial interaction

MC3T3-E1 (ATCC) cells (osteoblast) were cultured on the combi chips and kept in culture media made from α-MEM (Cellgro), with 10% FBS (ATCC), and 1% of Pen-strep (Cellgro) at 37$^{o}$C and 5% $CO_2$ [1]. The fluorescent stains used were blue nuclei stain (Hoecsht), and red F-actin stain (Rhodamine Phalloidine) provided by Molecular Probes. Detailed protocol was described elsewhere [53]. Imaging was done with Fluorescence Microscope (SPOT Advanced). Image analysis was performed with Image-Pro Plus Version 4.5.1.22 Media Cybernetics, Inc., an image processing tool.

#### 1.4.6. Statistical analysis

Statistical analysis was performed with Matlab ® Statistical Toolbox for ANOVA and T test. The tests performed were to check:

1. whether each sample was significantly different from the rest
2. whether each variable in the 2D combinatorial libraries significantly affected the result
3. whether there was any interaction of the two variables
4. whether the data for each point of interest in the combinatorial chip library was significantly different from the rest of data from the other points.

### 1.5. Hypotheses and Specific Aims

The hypotheses are:

1. Phase separation and difference in crystallization rates will create diverse microstructures and surface roughnesses on the surface which provide patterned size contrast in adhesive versus non-adhesive sub domain.
2. Surface properties can be used to control cellular behaviors included in surface receptor-initiated signaling pathways. The focus of this research will be limited to attachment density and cellular shape.

The specific aims are:

1. To use phase separation, dewetting, and crystallization of polymer blend films in a combinatorial method for material design purposes
2. To develop an optimum biodegradable and biocompatible polymer surfaces (microstructure and surface roughness) for controlling cell behavior (attachment density and cellular shape)
3. To obtain a correlation between the physical properties and the cellular behavior that can serve as a predictor for future designs.

# CHAPTER 2

# RESULTS AND DISCUSSION FOR POLYMER LIBRARY PREPARATION

## 2.1. Physical and Chemical Characterization

### 2.1.1. Confirming pattern of composition gradient

The pattern of composition gradient is confirmed by FTIR data.

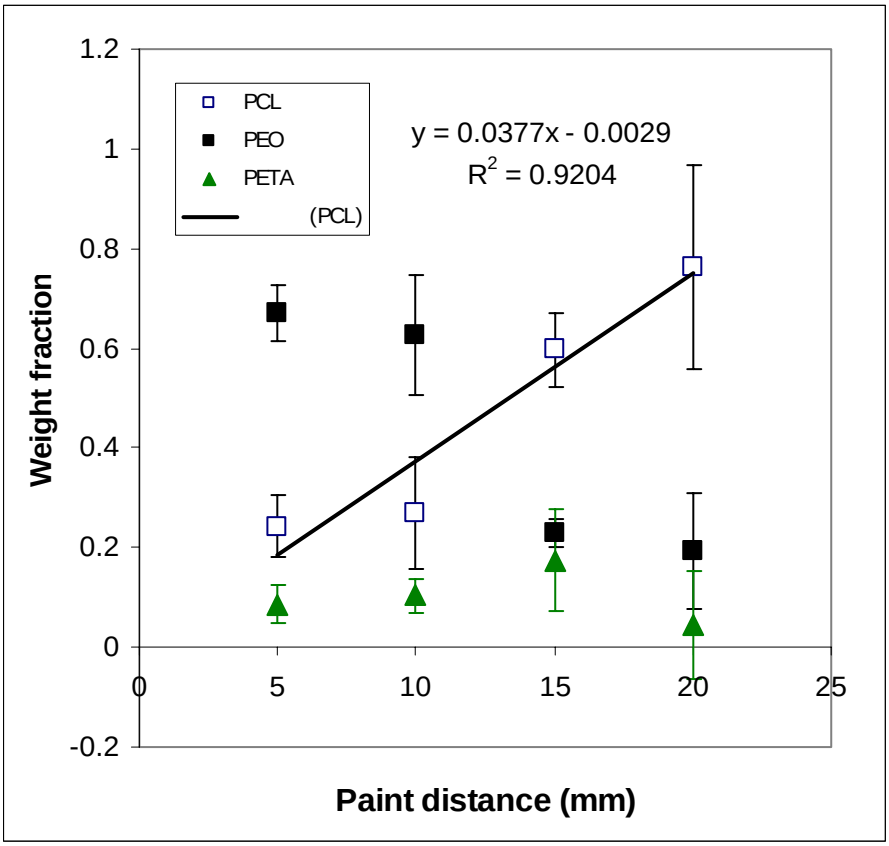


Figure 2. Data of weight fraction (φ) of the component as a function of paint distance (y) to confirm composition gradient on combinatorial samples.

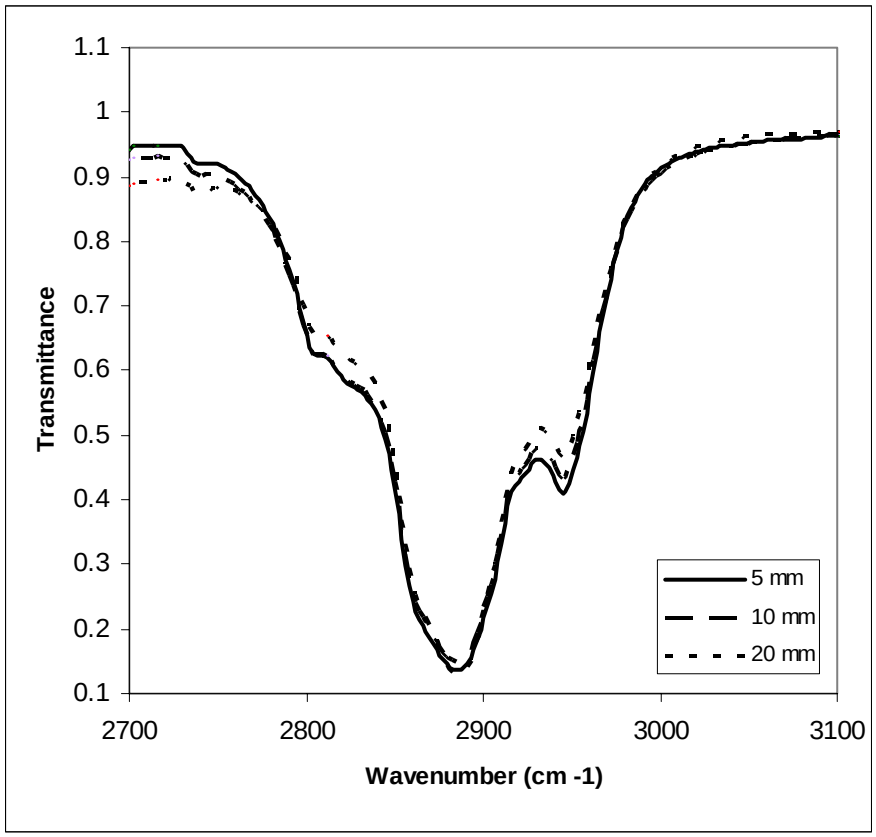


Figure 3. Sample of IR spectra showing gradual change from point to point at different paint distance.

2.1.2. Confirming linearity of thickness gradient

Thickness is measured with **Variable Angle Spectroscopic Ellipsometer (VASE)** at 3 positions in each sample. VASE measurement is very sensitive for surface non-uniformity (scattering). Since phase separation will increase surface roughness, therefore VASE measurement has to be conducted before annealing process.

The choice of the 3 measurement positions is based on the range that is free of distortions from the edges of coating process.

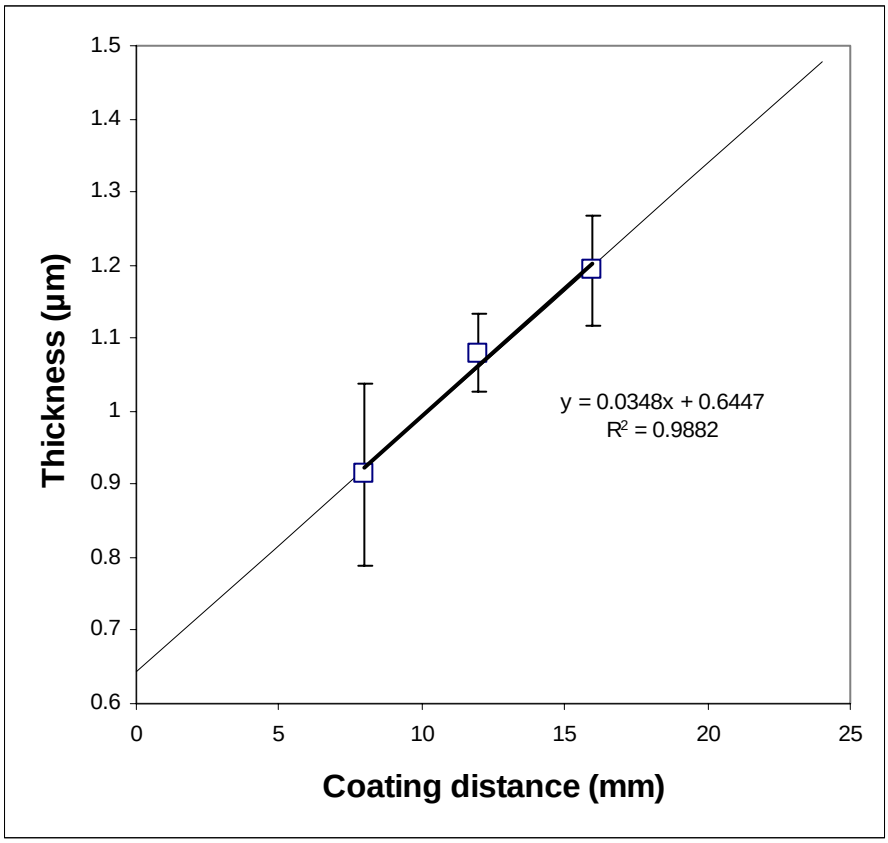


Figure 4. Thickness gradient confirmed with ellipsometer measurement.

Table 2. Extrapolated thickness value (h) for each coating distance (x) in the combinatorial chip.

| x (mm) | h (A) |
|---|---|
| 0 | 0.6447 |
| 4.8 | 0.811601 |
| 9.6 | 0.978502 |
| 14.4 | 1.145402 |
| 19.2 | 1.312303 |
| 24 | 1.479204 |

### 2.1.3. Confirming on Optimum Quenching Method

For the polymer blend films, steady state phase separated structure is reached after 2 hours of annealing process. At the end of the process, quenching is done to "preserve" the phase separated structure at each point in the combinatorial library. This determines the final supra molecular crystal structures of the polymer film. The local or primary crystal unit and packing changes have not been included in the observation yet.

Figure **5** shows that the crystal structure differs significantly for different quenching methods. This is due the crystability of cross linked PEG (to be explained in more details later in sub chapter 2.3) and PCL blend. Both polymer are crystallizable, but with different rate and different degree of crystallinity (Figure 6 and Figure 7). This difference can be **amplified** to make a greater **crystallinity contrast** between the two phases. Slow cooling or different quenching methods (i.e. at room temperature and at ice bath) show striking differences in crystal structure of the polymer. The difference in crystalline structure resulting from different quenching can be observed in Figure 5.

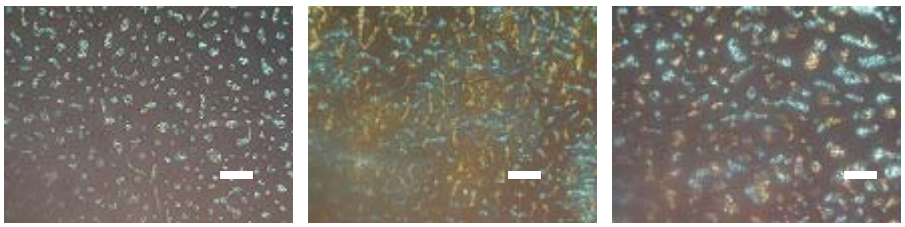

Figure 5. Crosspolarized Optical Microscope image taken at (h=0.98 um, T=100$^{o}$ C). Each image is 433.33 x 325 μm in size. Scale bar size is 50 μm. System: PEG-PCL blends film on Si wafer after annealing before immersion. From left to right: cooling rate 3$^{o}$ C/minute, quenching to room temperature, quenching to ice bath.

Spherulitic shape of PEG-rich sub domain as shown in Figure 6 can be explained by analogy to crystallization from concentrated solution. Spherulites are commonly formed from concentrated polymer solutions, and most frequently grow from the supercooled molten state. These growth patterns only occur from "privileged" nuclei, i.e. those that are capable of growing with a decrease in free energy (enhanced stability) to form ordered structure. In monodisperse polyethylene oxide, the growth rate of crystal in the melt depends on the crystal thickness, determined primarily by undercooling temperature [54].

To have a better understanding about the crystallization of the blend, it is good to observe the crystal structures (after annealing) of pure polymer first. Images of films from PEG, PEG crosslinked with MDI, and pure PCl at h=0.98 um, T=100$^{o}$C are given below.

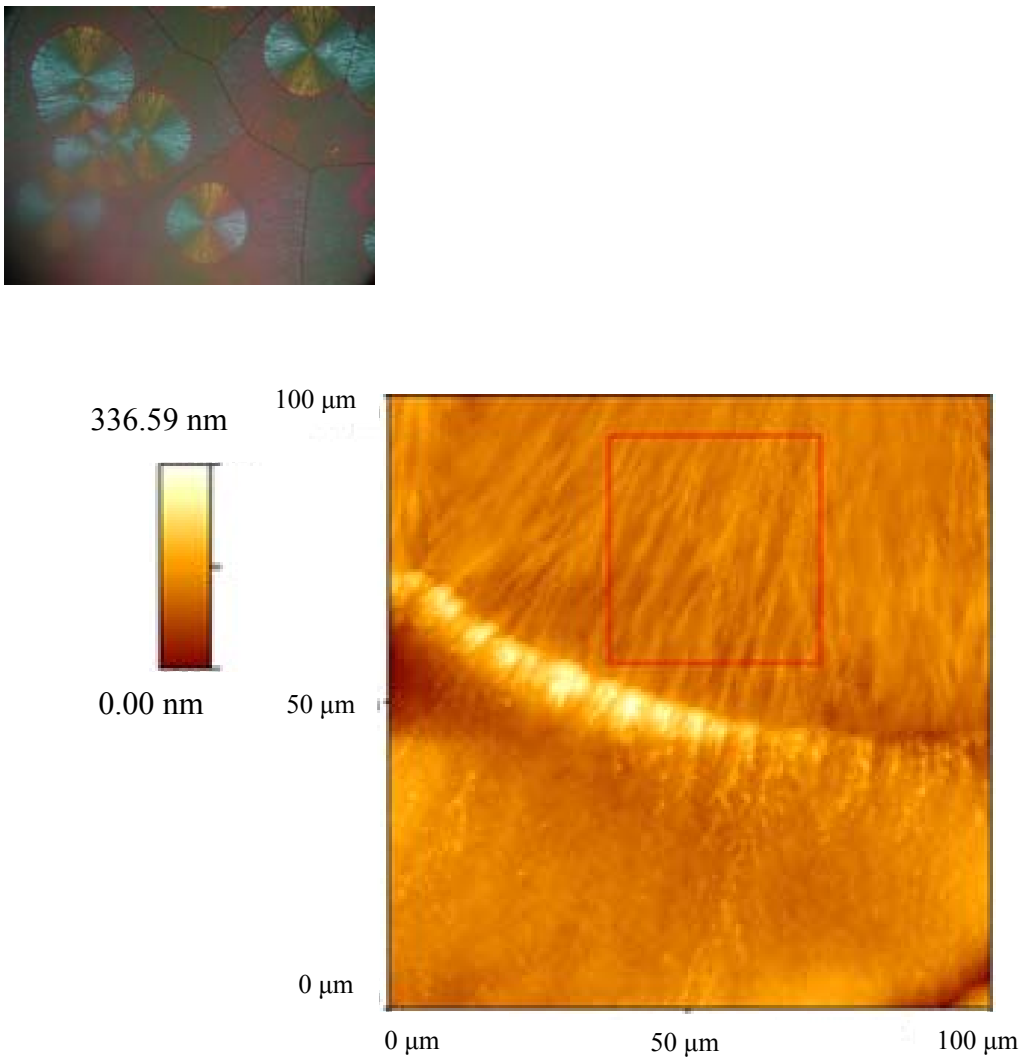


Figure 6. Crosspolarized Optical Microscope (top image, 433.33 x 325 µm in size) and AFM image analysis of PEG crosslinked with MDI (MDI to PEG mole ratio= 1 : 1.29).

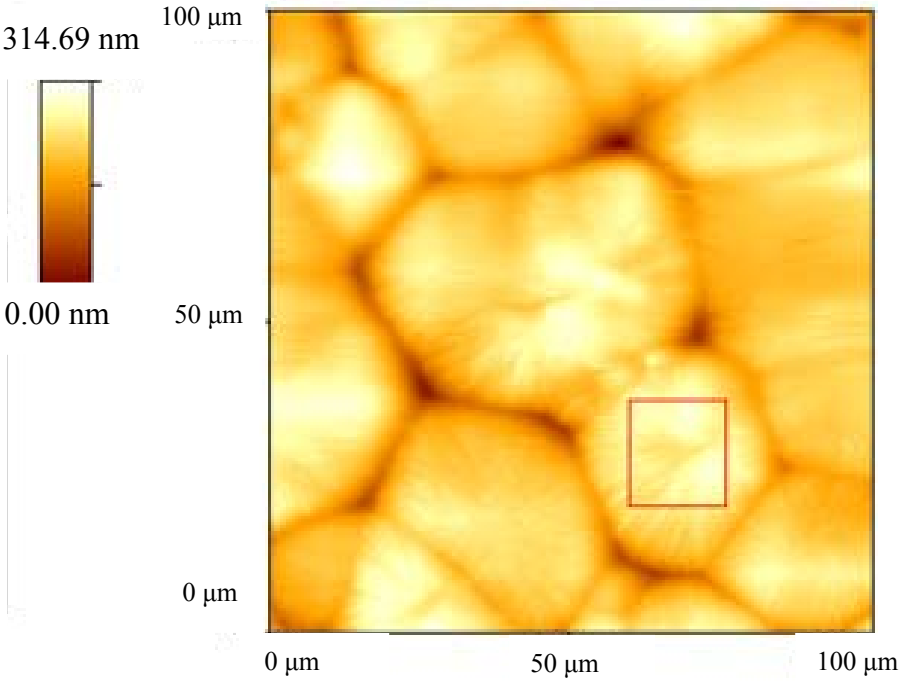


Figure 7. Crosspolarized Optical Microscope (top image, 433.33 x 325 µm in size) and AFM image analysis of PCL.

Table 3. Summary of AFM analysis on PEG-rich and PCL-rich sub domains.

| | PCL | | PEG | |
|---|---|---|---|---|
| | Overall | Inside spherulite | Overall | Inside spherulite |
| **Roughness** | 30.525 | 14.0509 | 18.6376 | 11.4134 |
| **RMS** | 40.0058 | 16.7145 | 28.4894 | 14.3377 |
| **Avg. Height** | 212.7963 | 259.6063 | 135.6497 | 130.0611 |
| **Max Range** | 314.688 | 84.483 | 336.591 | 107.28 |

It is clear from Figure 6 (top) that PEG crosslinked with MDI tends to be amorphous, and the existence of two areas with different crystallinities within one polygonized spherulite shows that there are two crystallization steps going on. Polygonized structures are produced when spherulites impinge upon each other, limiting forward radial growth. Growth rate is extremely temperature sensitive and generally believed to be nucleation controlled. Nucleation is termed primary for the onset of crystallization; the propagation of lamellae/spherulites (i.e. growth) is named secondary crystallization. Crystallization happening after the radial growth ceases (densification/"filling in") follows this step had been reported before by dilatometer, and it happened inward to the center [55].

From previous studies, it was proven that crystallization proceeds outward from a primary center (a nucleation site) until growth is arrested or slowed into an imperceptible level. High supersaturation leads to spherical arrays, which are comprised of radiating platelets or lamellae (often splayed and branched) in which the polymer chains also folded depending upon molecular weight and experimental condition. The polarizability of a spherulite is much greater along its chain axes than it is transverse to them, but still it shows positive birefringence since there is a highly polar side in the polymer chains [49].

Figure 7 shows that PCL has the characteristic of having elevated islands with smaller structure size than the spherulites of PEG. Based on these two pure polymer crystal structures at micrometer thickness, the phenomenon of phase separation of the blend as shown in Figure 5 can be better understood.

As shown in Figure 6, Figure 7, and Table 3, PCL-rich sub domain is rougher and more crystalline than PEG-rich sub domain. Therefore crystallinity is related to the roughness of the two sub domains.

From these results, it is shown that difference in quenching method affects crystallinity. Degree of crystallinity affects microstructure and surface roughness. Therefore, it is decided that the optimum method to amplify crystallinity contrast is by quenching to ice bath.

Comparing the images in Figure 5, quenching at room temperature versus at $0^{o}$ C creates a striking difference in crystal structure, but the spherulitic size is retained. This supports the assumption that phase separation was properly 'frozen' by quenching.

## 2.2. Biomaterial Surface Properties Library: PEO-PCL with PETA crosslinker

PEO needs to be crosslinked because it still dissolves in water even at high molecular weight. The time scale for dissolution is much shorter than the time needed for the cell culture and bioassays. Weight loss due to dissolution is more than 50% within overnight immersion in water at $37^{o}$C. The weight loss can be reduced to less than 10% with PETA crosslinking[8].

[8] At PETA concentration 10% of total PEG-PETA solution in chloroform and annealing temperature: $65^{o}$ C.

The mechanism of crosslinking using acrylate with UV exposure is to create reactive radicals at C=C functional group from acrylate and at C=O functional group from PEO to form crosslinks [52].

One additional problem related to dissolution in water is that the hydrophilic PEO content caused the film to peel off from Si wafer surface. To deal with this problem natural silicon oxide layer on the Si wafer is removed by etching such that Si surface hydrophobicity increases. This way, surface hydrophobicity is optimized for better film adhesion on Si wafer surface using the interplay of attractive force between hydrophobic surface and PCL and between water and PEO chains in the blend. But there is a possibility of interfacial interaction with Si surface related to the phase separation observed. It has been reported recently that surface and interfacial forces can penetrate up to 500 nm thick polymer blends film [56].

The result of crosslinking PEO with UV was unsatisfactory in several aspects.

a. Trade-off between preventing loss of PETA crosslinker and preventing PETA from changing the phase separation pattern. If UV exposure is done after annealing, some portion of unreacted PETA will be lost in the thermal treatment or unreacted PETA might react with functional groups other than the ones on PEO chain-ends. But if UV exposure is done before annealing, introduction of crosslinks affect phase separation pattern of PEG and PCL. This effect can be observed by comparing Figure 8 to Figure 9. It is highly possible that phase separation pattern is affected partially because UV exposure crosslinks both PCL and PEO.

b. Loss of adhesive and non-adhesive contrast. PCL is theoretically more reactive to acrylate than PEG, because of the existence of C=O functional group in PCL. The UV exposure activates free radicals throughout the whole sample. After UV is turned off, the radicals are not present anymore. But they might react with oxygen or moisture to form polar surface group. This disturbs the adhesive/non-adhesive patterning.

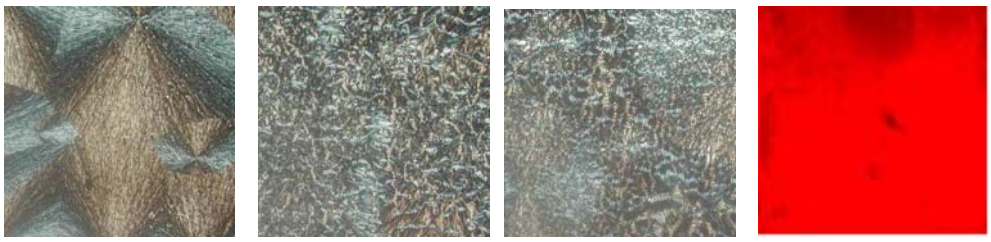

Images of point 1, 5, and 9 zoomed and Fluorescence Microscopy image of point 5 after Fibronectin coating (each image is 160 x 160 um in size)[9].

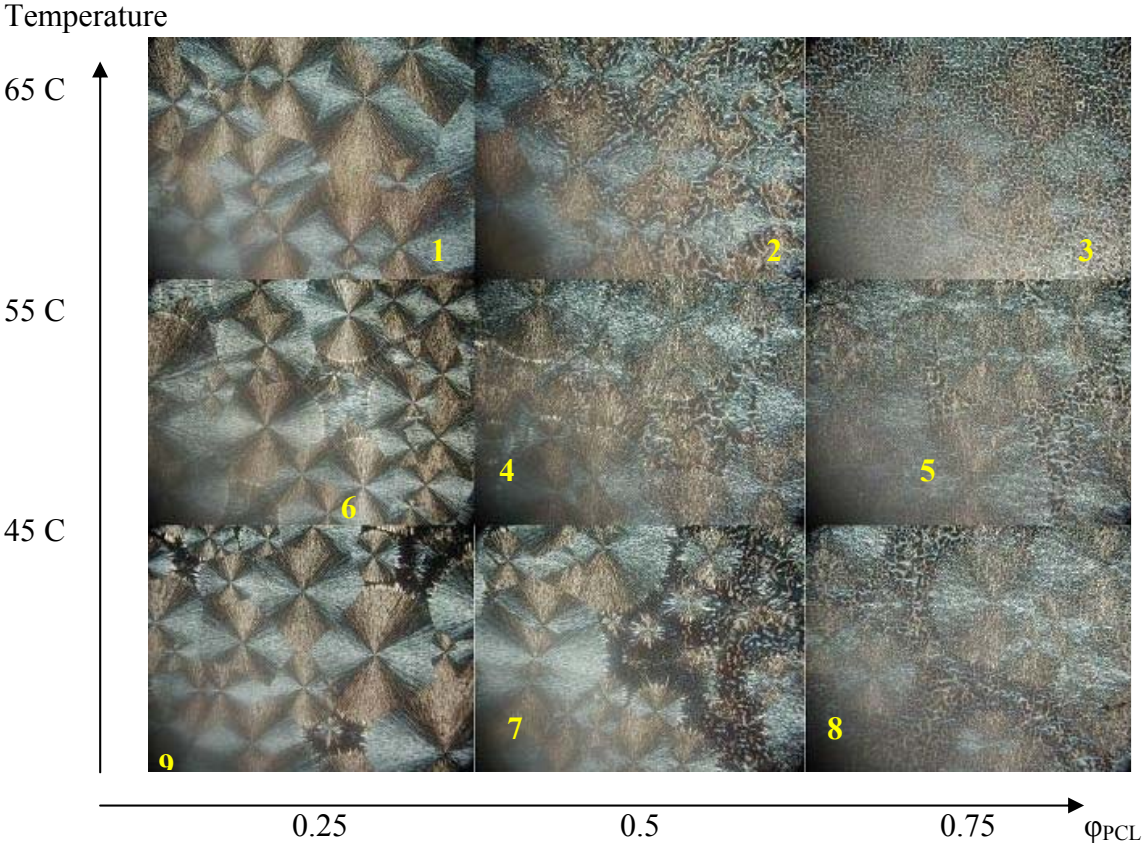


Figure 8. Combi chip PEO-PCL crosslinked with PETA after 2h annealing (each image is 433.33 um x 325 um in size). PETA content is 10% wt. of total solution PETA-PEO in chloroform.

[9] Numbering and ($\varphi_{PCL}$,T) value at each point correspond to lower part of Figure 8.


Pure PEO

Temperature

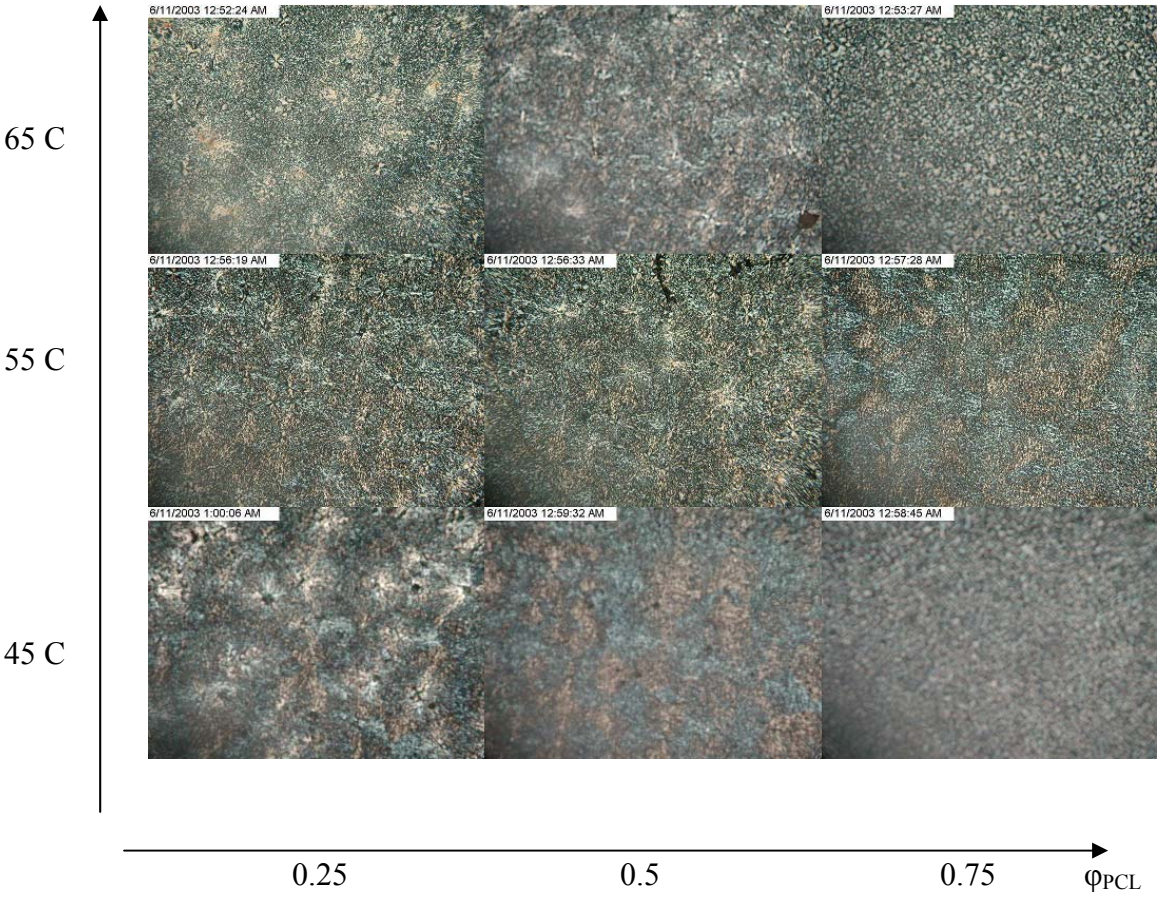


Figure 9. Combi chip PEO-PCL without PETA after 2h annealing.

## 2.3. Biomaterial Surface Properties Library: PEG-PCL with MDI crosslinker

### 2.3.1. Chemistry of crosslinking reaction

The mechanism of crosslinking with MDI is by creating a **polyurethane** bond at the -OH group at the ends of PEG chains[57].

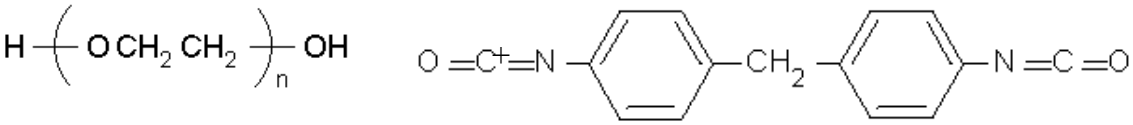

⇨ H –(- O-CH2 – CH2 -)-O – **CO –NH** – phenyl – CH2 – phenyl –**NH – CO** -)$_n$ –

Figure 10. Reaction diagram for MDI crosslinking through polyurethane bonds.

In addition to chemical crosslinks by polyurethane bonds, an additional physical polymer network is created. In this network, hydrogen bonds form between urethane bonds chains align, leading to crystalline hard domains that act as physical crosslinks. This contributes to the gelation of the crosslinked polymer.

The problem of peeling and dissolution of PEG in water was resolved by maintaining the optimal the ratio of excess MDI to PEG. The result of the optimization is shown below.

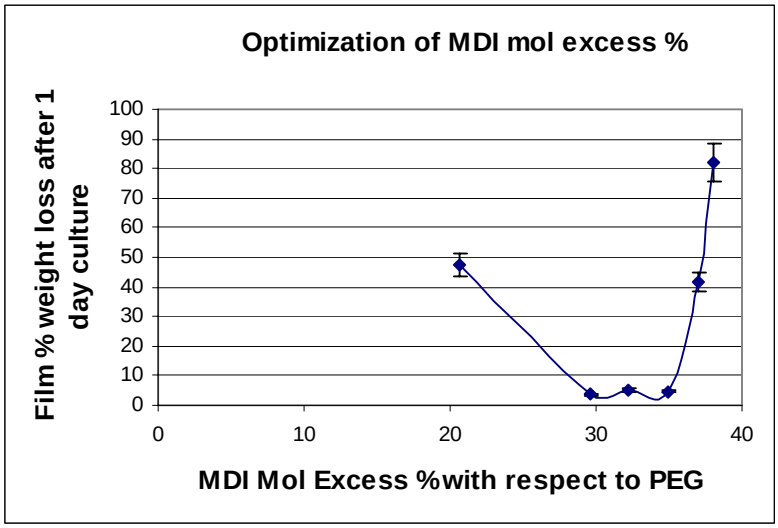


Figure 11. Optimization of MDI to PEG mole ratio for optimum film weight retained on the Si wafer surface after immersion into aqueous media.

2.3.2. Background for replacement of composition gradient with thickness gradient

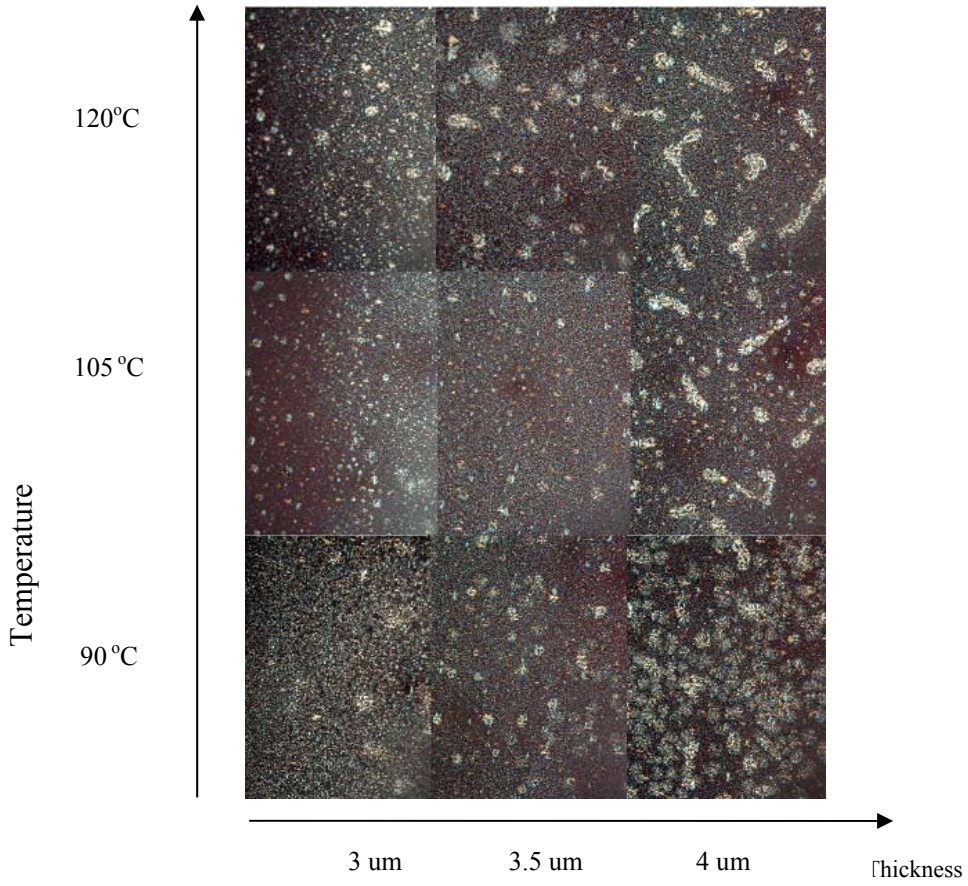


Figure 12. Cross-polarized optical microscopic images of PCL-PEGPU libraries (each image is 325 um x 433.33 um in size) coated on Si wafer with 15 minutes etching and uniform $\varphi_{PCL}$=0.2 (MDI to PEG mole ratio = 1 : 1.1).

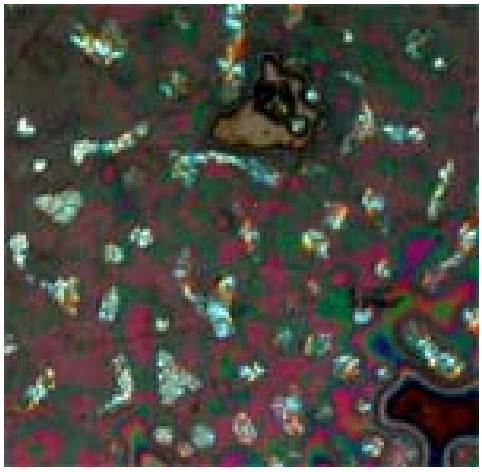

Figure 13. Blown up crosspolarized optical microscope image of 108 x 108 um size, taken from point 5 in Figure 14.

From the results presented above, a BOE etching period of 15 minutes formed the features mostly due to dewetting rather than from phase separation.

When BOE etching time is increased to 25 minutes, the hydrophobicity of the Si wafer improves further and the phase separation pattern shows a strikingly different result. Dewetting is eliminated even with film at half of the initial thickness (compared to Figure 12 and Figure 13).

Dewetting can be explained by the hydrophobicity of the polymers and the Si wafer. At high polymer hydrophobicity, wetting free energy becomes positive and film breaks into holes and droplets. But, upon immersion in water, the polymer will continue to stay intact onto the surface due to the presence of strongly hydrophobic PCL.

It can be observed from Figure 13 that dewetting process is involved in creating phase separated structure and that the crystalline part of the phase separated structure is comprised of single phase crystalline area. Polymer crystals generally consist of two phases, i.e. solid region and liquid region. Liquid region is responsible for the amorphous part of the structure. Dewetting is shown to increase the portion of amorphous part. Dewetted area can not crystallize properly because dewetting reduced the thickness of the film at that point. The effect of dewetting to film thickness and crystallization has been observed in some previous studies [58, 59]. Therefore gradient for combinatorial library exploration was later shifted into thickness (h) instead of composition gradient.

2.3.3. Microstructure library

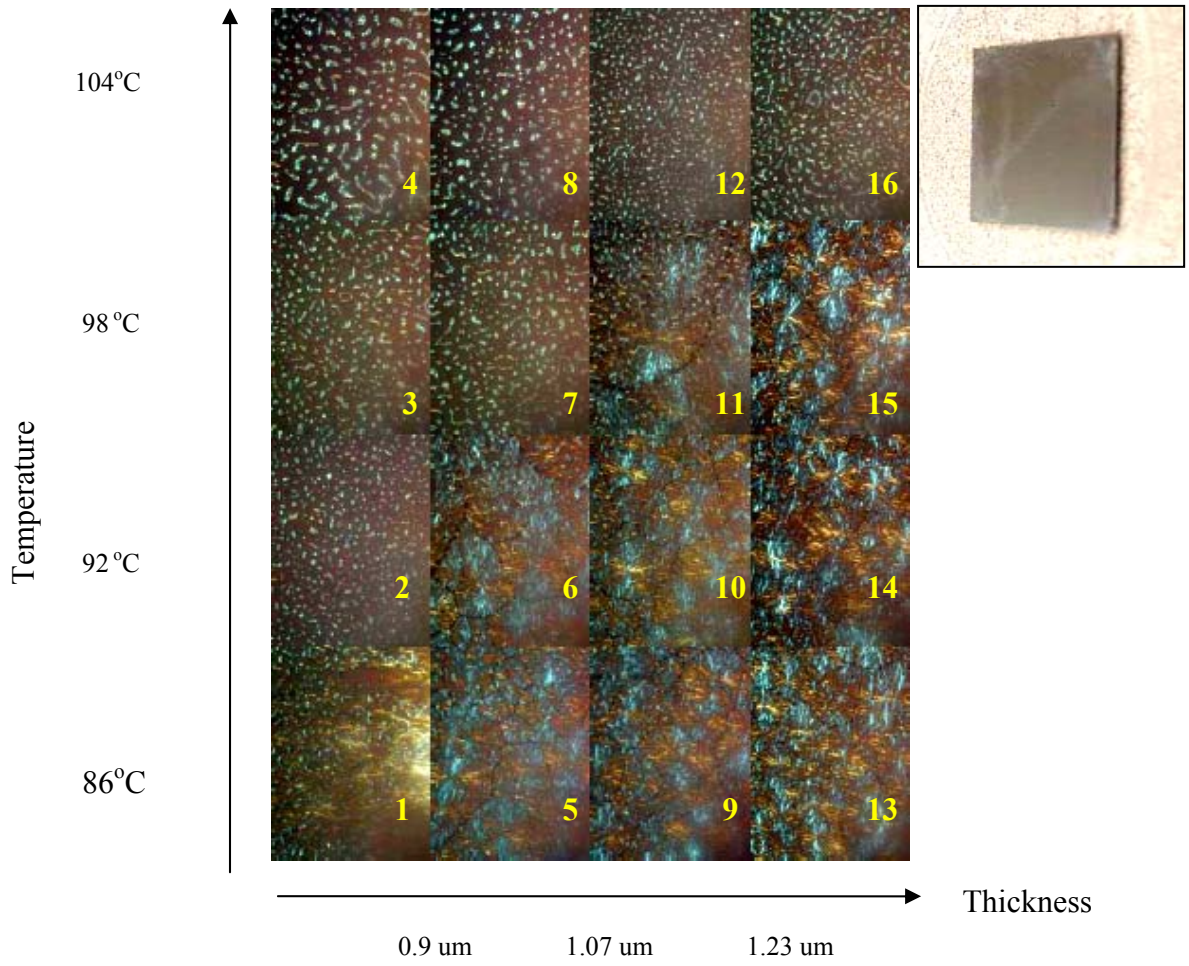


Figure 14. Crosspolarized Optical Microscope image[10] of PEG/PU-PCL library with BOE etching 25 minutes, MDI to PEG mole ratio= 1 : 1.29 and $\varphi_{PCL}$=0.22. (each image is 325 um x 433.33 um in size). Insert: full 24 x 24 mm sample picture taken with regular camera.

[10] Blade coating is in the direction of going from point 1 to point 13. Similar position or image numbering with reference to combinatorial libraries is consistently used in the subsequent chapters.

Figure 14 shows the sample divided into two triangular halves. Looking at the inserted image, the top half appears transparent while the bottom one is hazy. Comparing the insert with the cross polarized Optical Microscope image, the transparent part corresponds to a more amorphous part of the film, i.e. the part with larger portion of dark area. This is true especially in PEG-rich sub domain (the background spherulites). It can be concluded that annealing at higher T and coating a thinner film tends to give a more amorphous PEG-rich sub domain.

The possible explanation is that "freeing" the whole chains of crosslinked PEG at ordering process during crystallization requires energy. For thicker film, more thermal energy is required since more chains need to be moved. Hence a higher temperature is needed to create a similar crystallinity, than in the thinner part of the film. Further research needs to be done to further examine this aspect.

Figure 14 shows larger PCL-rich sub domain formed at higher T and thinner film. The explanation of this follows the same fashion of PEG-rich sub domain's structure formation described previously.

The improved crystallinity contrast between PEG-rich and PCL-rich sub domain in high T thin h area can be explained as follows. The thicker the film means there are more chains to be moved in order to create a certain contrast level. Hence, more energy is needed. This is why higher temperature gives a better contrast. Furthermore, with 25 minutes etching, PEO sticks to the surface better. Therefore, it needs more energy to get the chains off the surface. The critical point is along the dividing line of the two halves in Figure 14.

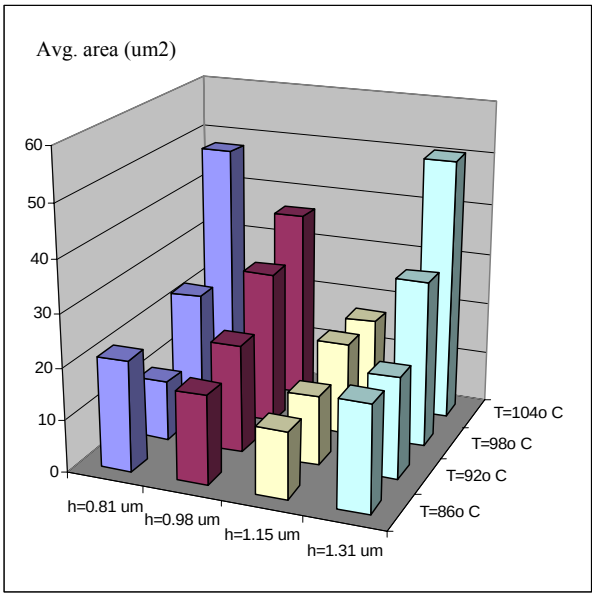


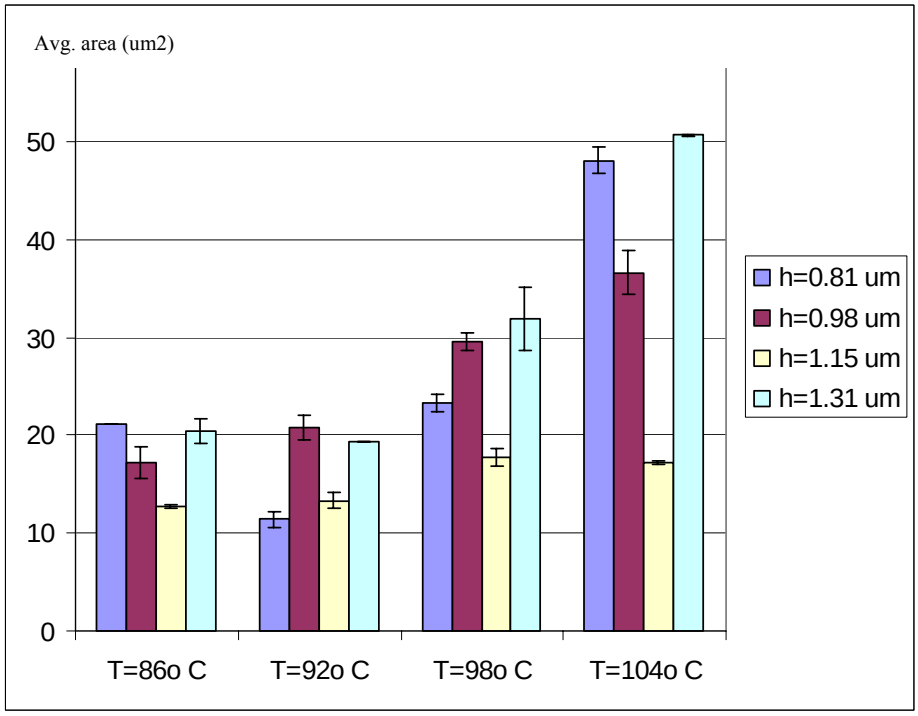


Figure 15. Microstructure patterning map of combinatorial chip corresponding to Figure 14.

Figure 15 describes the percentage of PCL-rich sub domain over the total area of two sub domains. Generally, microstructure showed a finer pattern of PCL-rich islands at lower T. The explanation follows a similar fashion with that of finer PCL-rich sub domain at higher T and thinner film described previously. To summarize, more energy per polymer chain is available at higher temperature and thinner film. Therefore, better chain orientation is possible at high T and thin film, i.e. bigger features are created.

The correlation of feature size and thickness shown in

Figure **15** shows mixed trend. This could be due to the possibility that the first and last row of the chip could have some errors resulting from the edges of coating point, or due to two (or more) opposing forces for chain movement. For example: polymer-surface interaction prevents the movement, so the thinner the film is, the finer features tend to appear; on the other hand, thinner film will have a smaller **vertical** temperature gradient, so the accessibility of energy for chain movement will be larger in thinner films, i.e. bigger features tend to appear in thinner film.

### 2.3.4. Surface roughness library

A closer observation of the part with lower T and thicker film reveals the dewetting on the perimeters of spherulitic features, and phase separation into bilayers [60]. Another interesting point is that for the same T and h gradient, the roughness in the sub domains shows different features (compare roughness of PCL-rich to PEG-rich sub domains in Figure 17 and Figure 20, summary in Table 4). Furthermore, the degree of morphological change after immersion into water differs significantly for each subdomain (compare roughness of PCL-rich to PEG-rich sub domains in Figure 17 to Figure 18, and Figure 20 to Figure 21, summary in Table 4 and Table 5).

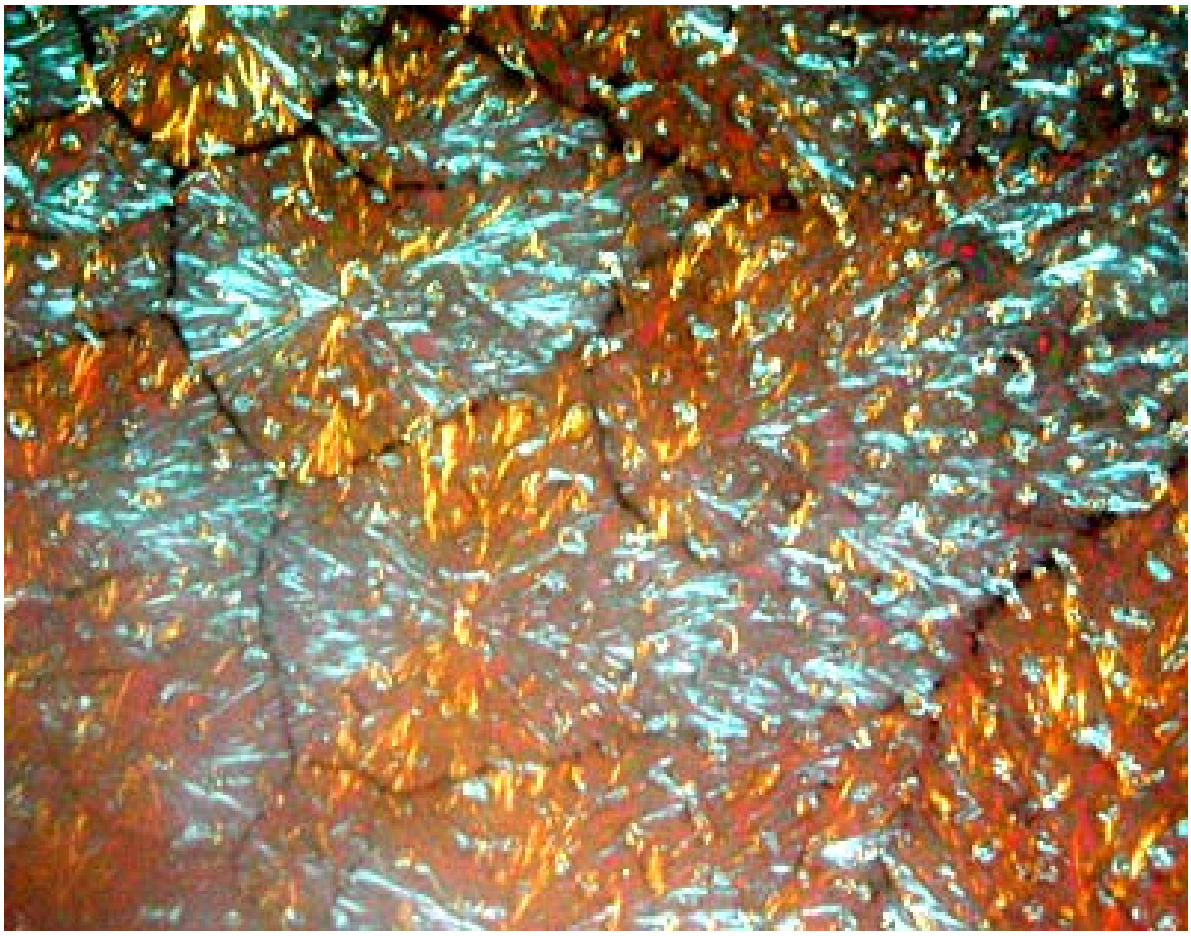

Figure 16. Crosspolarized optical microscope image of PEG-PCL blend film on Si wafer after annealing before immersion, corresponds to bottom half (hazy part) of Figure 14. (h=0.98 um, T=92$^{o}$ C).

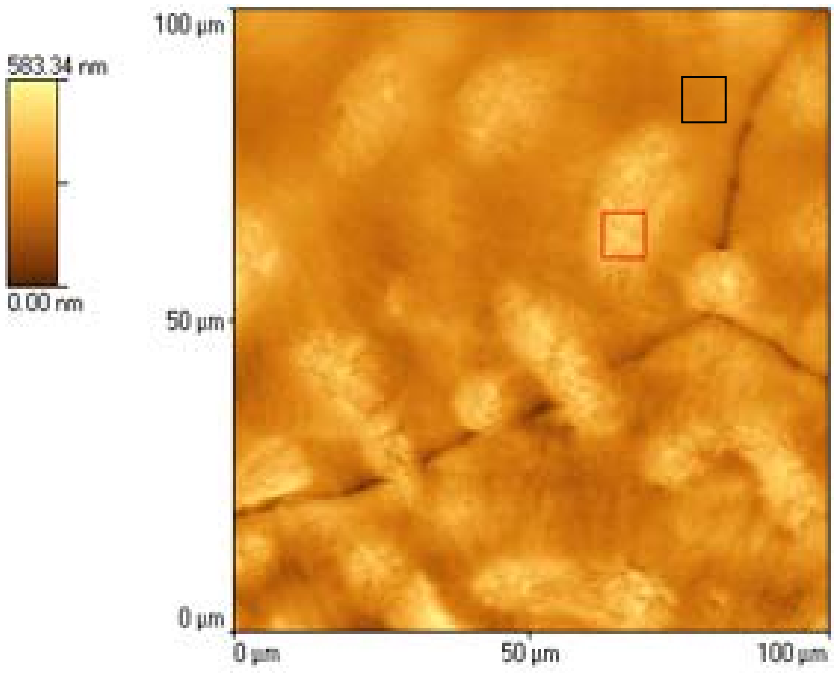


Figure 17. AFM image of PEG-PCL blend film on Si wafer after annealing before immersion, corresponds to point 6 from bottom half (hazy part) of Figure 14. (h=0.98 um, T=92$^{o}$ C). Surface properties in the red square boundary (PCL-rich islands) and black square (PEG-rich spherulitic feature) are listed in Table 4.

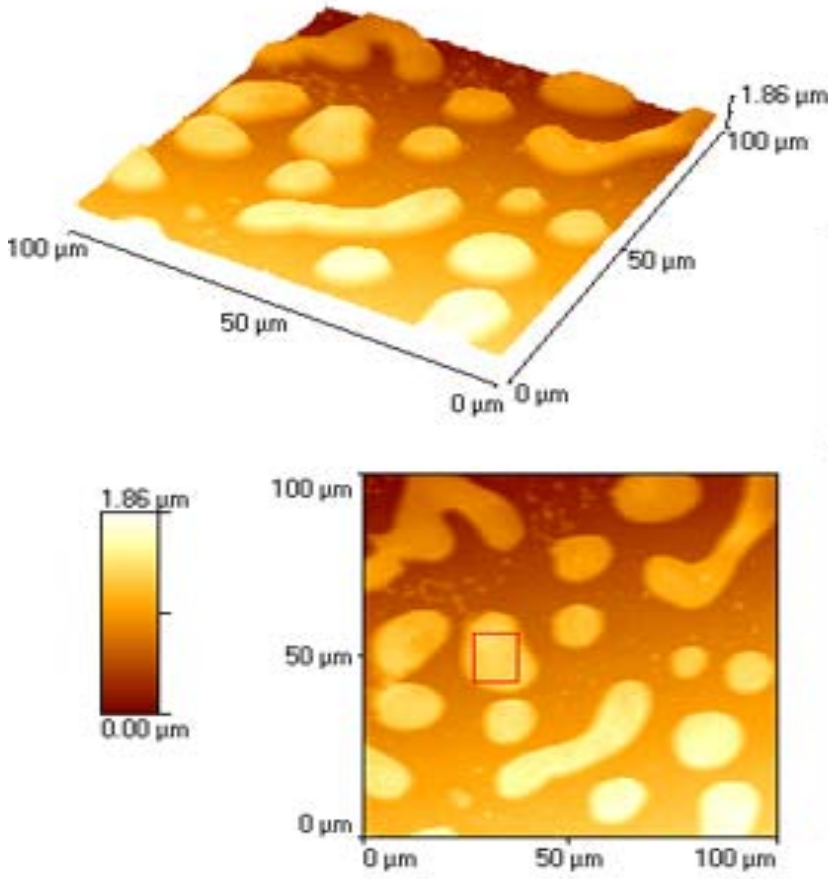


Figure 18. AFM image of PEG-PCL blend film on Si wafer after annealing after 2 d immersion into deionized water at 37$^{o}$C, corresponds to point 6 from bottom half (hazy part) of Figure 14. (h=0.98 um, T=92$^{o}$ C). Properties of each sub domains are listed in Table 5.

In the AFM image Figure 17, we can see that the lower layer (background) with big spherulitic pattern is topped with another phase as the island features. The different compounds in each phase detected are by phase imaging and internal sensor measuring the interaction force between the AFM cantilever tip and the surface. Corresponding crosspolarized optical microscope image shown in Figure 16 shows the polygon structure of the PEG-rich spherulites as the background of PCL-rich islands. The AFM image clearly shows that the phase separation is vertical (top and bottom layer), confirming the visible peeling off of scratched film upon immersion into water. This is in accordance to the Optical microscope image of the two layers in Figure 13.

After immersion, the PEG layer lost its spherulitic structure. The AFM image in Figure 18 confirms this. Dissolution of PEG caused surface roughness to increase.

At the higher annealing temperature and thinner part of the film (top-half, transparent part of Figure 14), we will observe different surface properties.

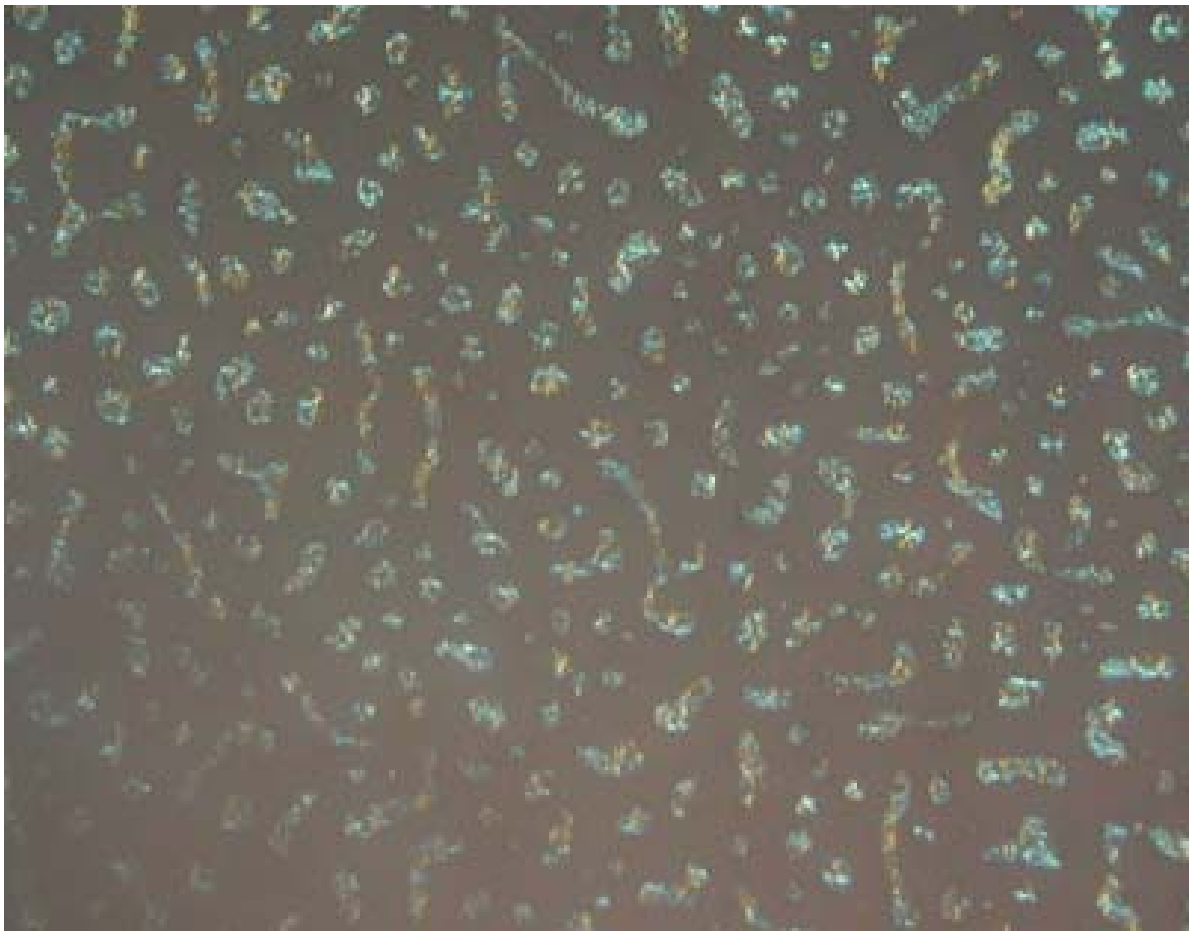

Figure 19. Crosspolarized optical microscope image of PEG-PCL blend film on Si wafer after annealing before immersion, corresponds to point 7 from top half (transparent part) of Figure 14. (h=0.98 um, T=98$^{o}$ C).

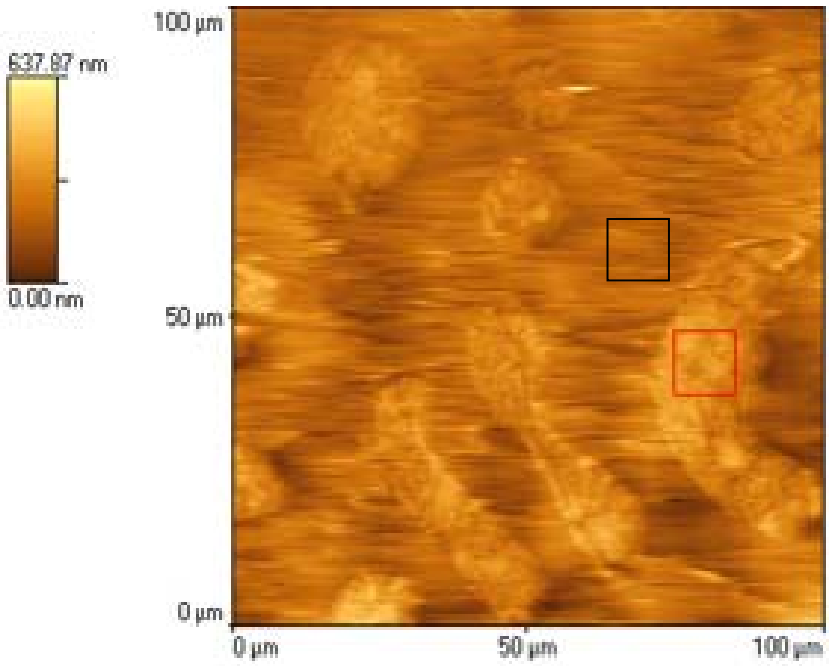


Figure 20. AFM image of PEG-PCL blend film on Si wafer after annealing before immersion, corresponds to point 7 from top half (transparent part) of Figure 14. (h=0.98 um, T=98$^{o}$ C). Properties in the red square boundary (PCL-rich islands) and black square (PEG-rich spherulitic feature) are listed in Table 4.

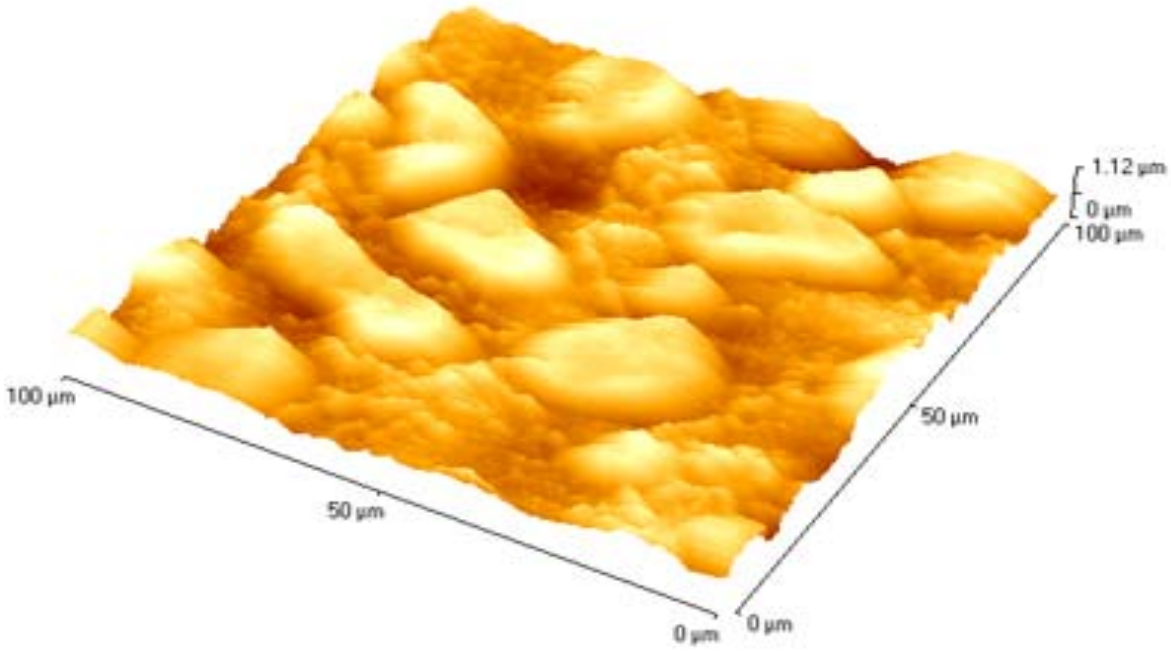


Figure 21. Crosspolarized optical microscope image of PEG-PCL blend film on Si wafer after annealing after immersion, corresponds to point 7 from top half (transparent part) of Figure 14. (h=0.98 um, T=98$^{o}$ C). Properties of each sub domain are listed in Table 5.

Table 4. Summary of surface roughness (nm) as a comparison between sub domains at two different halves of the sample, i.e. point 6 and point 7, corresponding to Figure 14 before immersion.

| | PCL-rich island | St. Dev | PEG-rich spherulite | St. Dev | Whole image | St. Dev |
|---|---|---|---|---|---|---|
| **Point 6** | 75.15 | 68.92 | 57.07 | 60.49 | 102.79 | 106.38 |
| **Point 7** | 42.62 | 12.14 | 51.88 | 39.34 | 86.96 | 66.11 |

Table 5. Summary of surface roughness (nm) as a comparison between sub domains at two different halves, i.e. point 6 and point 7, corresponding to Figure 14 after immersion.

| | PCL-rich island | St. Dev | PEG-rich spherulite | St. Dev | Whole image | St. Dev |
|---|---|---|---|---|---|---|
| **Point 6** | 142.66 | 114.12 | 119.77 | 44.44 | 210.84 | 72.81 |
| **Point 7** | 37.32 | 32.79 | 102.13 | 10.04 | 157.30 | 60.54 |

The microstructures before annealing and after annealing show similar patterns, but surface topography changes drastically.

The summary of surface roughness patterning combinatorial libraries on the whole chip scan can be examined in Figure **22**, Figure 23, and Figure **24**.

Furthermore, results show that cells are sensitive to surface roughness and phase-separated microstructure upon their adhesion on the surface. This is demonstrated in the results in chapter 3. Cells preferentially adhere on the area with intermediate to high

surface roughness, corresponding to higher T and thinner part of the film (top-half, the transparent part of Figure 14).

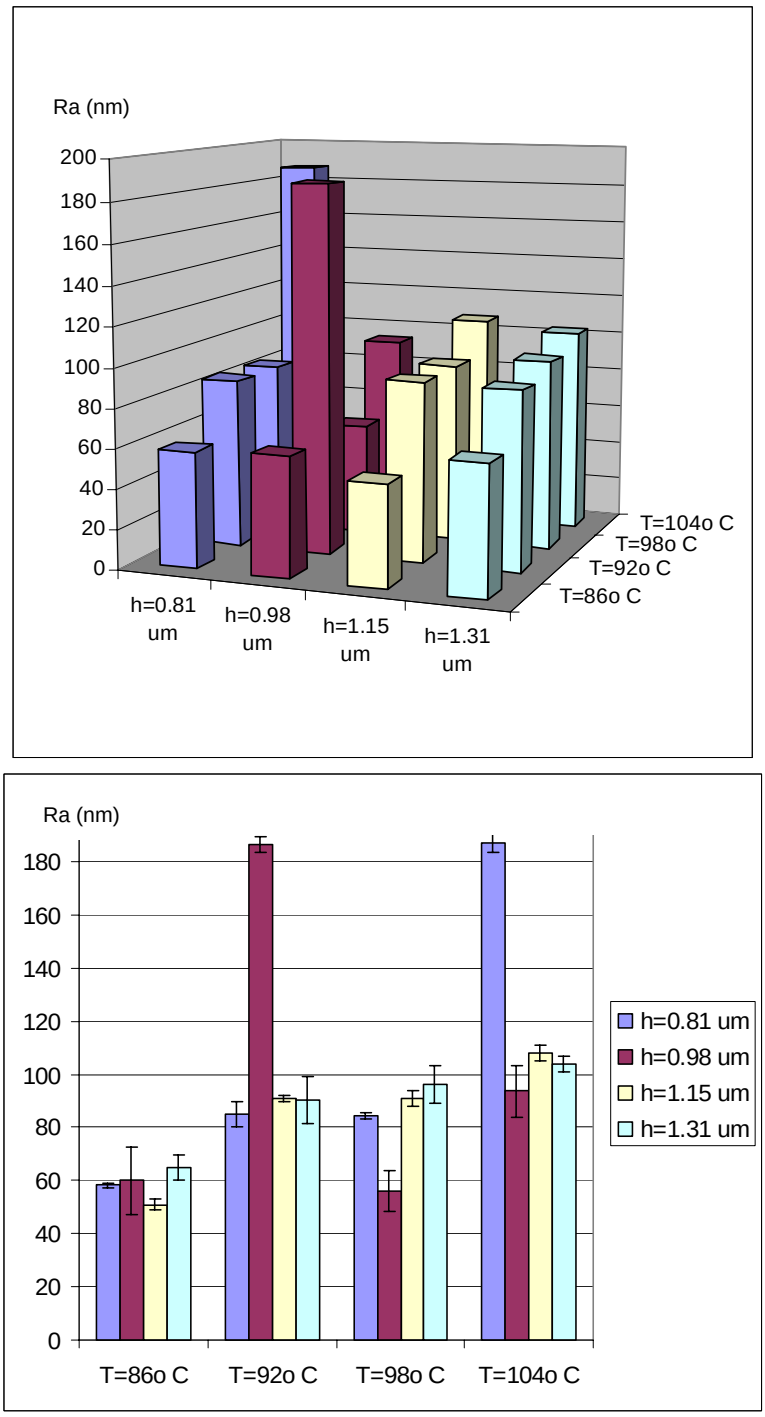


Figure 22. Library of Surface Roughness for PCL-rich sub domain of combinatorial chip corresponding to Figure 14 [11].

[11] All points are significantly different at 95% confidence interval to at least 6 other points.

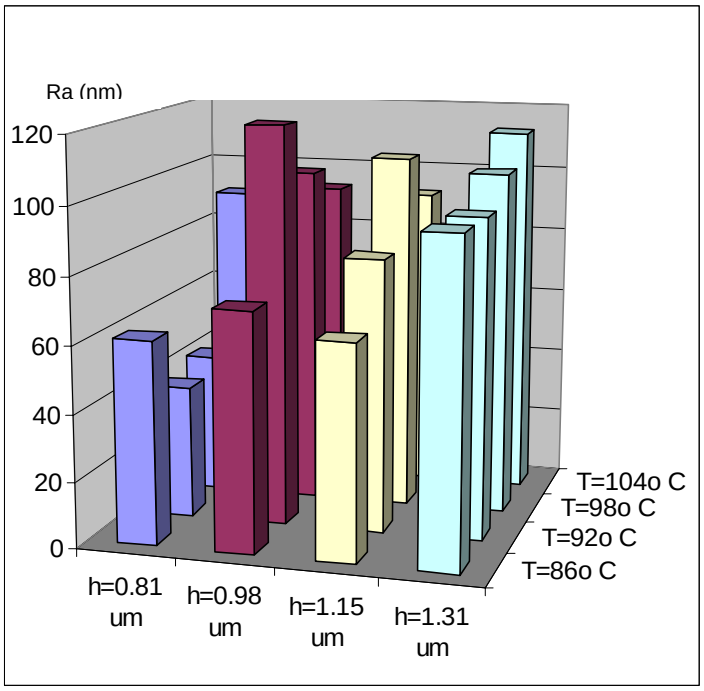


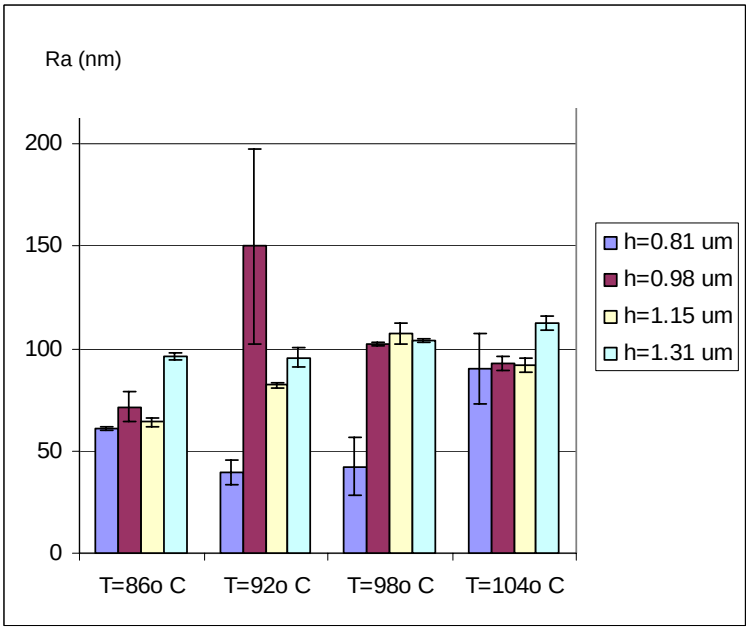


Figure 23. Library of Surface Roughness for PEG-rich sub domain of combinatorial chip corresponding to Figure 14[12].

[12] All points are significantly different at 95% confidence interval to at least one other point.

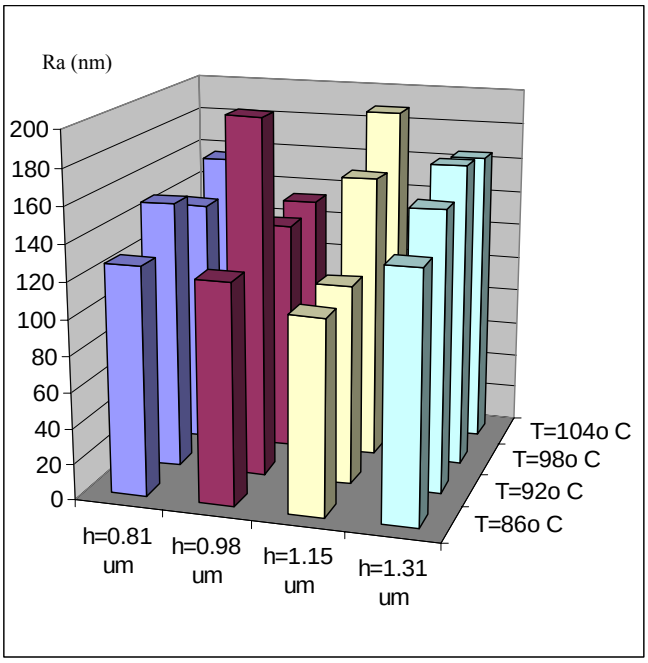


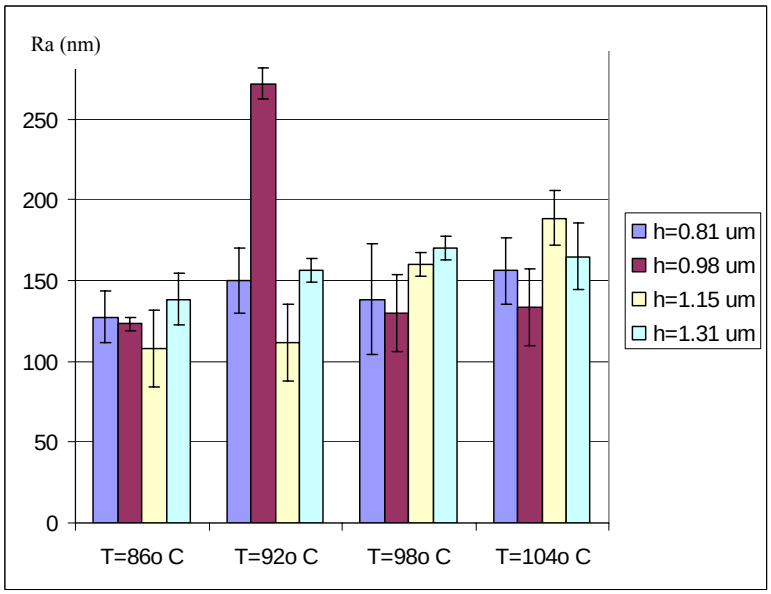


Figure 24. Library of Overall Surface Roughness from combinatorial chip corresponding to Figure 14[13].

[13] All data points are significantly different at 95% confidence interval from at least one other point, except point 11.

Results show that surface roughness in PEG-rich sub domain are more uniform, compared to that of PCL-rich sub domain. The trend of overall surface roughness is increasing as T is higher and film is thinner.

### 2.3.5. New Points of Interest

The most interesting new features are:

1. The existence of **bilayers** created simultaneously by a **single** coating. PEG rich phase retains the big-spherulitic feature while the PCl-rich layer forms the small islands. Judging qualitatively from the intensity of cross polarized optical microscope images, PCL-rich sub domain has a higher crystallinity than the PEG-rich spherulitic background. The bilayers are observed by immersing the surface-defect (scratched) into water. It can be clearly seen that the top layer is PCL and the bottom one is PEG-rich layer (Figure 17).
2. The amplification of temperature and thickness gradient on surface roughness by immersion. This is explained previously in sub chapter 2.1.3.

The possible explanation for the existence of simultaneous bilayers structure created upon phase separation can be explained by the tendency of surface with lower energy (larger contact angle) tends to be repelled by the solid surface (Si wafer as the substrate). Hence, it is reasonable to see the result of PEG-PCL blend film as pseudo two layers. It is inferred from the results above that the crystalline phase is the PCL-rich phase (bright islands in Figure 4), exposed at the elevated features in the phase separated structure; while the less crystalline phase as the background is PEG-rich phase (dark spherulitic features in Figure 4).

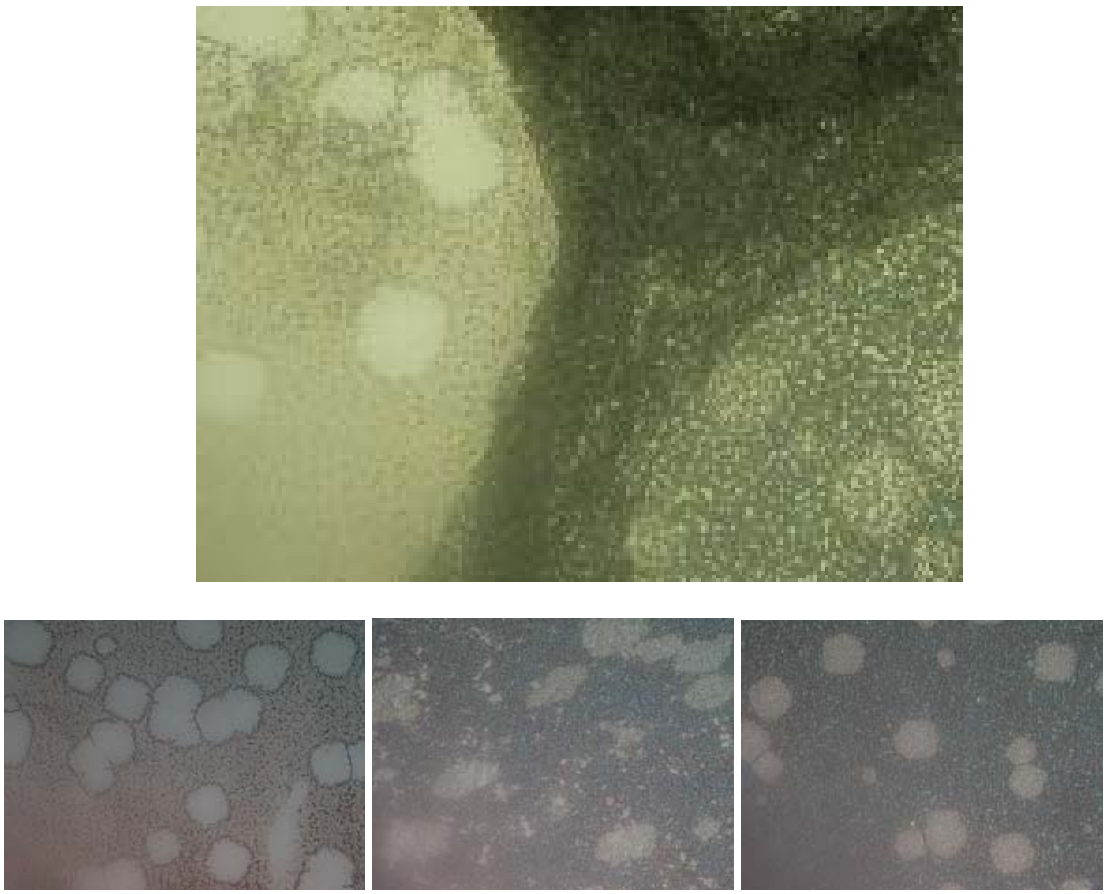

Figure 25. Crosspolarized optical microscope image of PEG-PCL blend film with defect on the film to peel the layers after immersion in water before annealing step
a. left part: silicon wafer exposed, right part: top and bottom layer intact (notice difference in color represents the thickness of the film and the pattern of islands on the right part represents the top layer of PCL-rich sub domains appearing as islands sitting on top of spherulites of PEG-rich sub domains)
b. bare silicon with PEG-rich spherulite sub domain remains
c. bottom layer with finer holes created by dissolution of PEG chains into water
d. top layer of PCL-rich sub domain showing clearer bluish and brownish color representing a more crystalline phase captured in crosspolarized image.

The microstructure resulting from phase separation is partially affected by surface effect (only to the lower layer of the film; the spherulitic feature is partially interacting with Si surface, affecting the temperature required to move the chains to free themselves from the quenching history upon film coating and solvent evaporation). But the phase separation between top and bottom layer is purely 3D case, the area/size/shape and distribution of PCL islands is not affected by thickness, only by temperature.

We can observe from Figure 6 that the bottom layer is split further into two parts, the part that is affected by interaction with silicon chip (the one that stays as "left-overs" upon peeling) and the part that is unaffected (free to dissolve). But they are interacting with each other when peeling force (from immersion) is absent on the period when they are annealed (to free the chains and get rid of history). It is shown in the images above that Figure25d has higher crystallinity (PCL-rich top layer) than

Figure 25c (PEG-rich spherulitic structure). Figure 25b shows only the 'left-overs' from the peeled off bottom layer, this is the part that interacts the most with Si wafer surface.

## 2.4. Conclusion

The result confirmed that phase separation and difference in crystallization rate create desired microstructure and surface roughness libraries. Library for microstructure is more reliable than that of surface roughness, judging from the p value of multi comparison statistical T test.

The contrast provided in the library encompasses that of adhesive versus non-adhesive and surface roughness at overall and sub domain level.

As a summary, bigger microstructure and rougher surface is achieved at higher T and thinner film.

## 2.5. Future Improvement Plan

Up to this point, no combinatorial technique has been applied to check on mechanical properties of the biomaterial, while actually the cell is reported to "sense" this particular property of a surface upon adhesion [24].

Microstructure spacing is still left unexplored in this result. Quantitative analysis is needed to have a better description of surface properties library.

To understand the exact surface properties sensed by the cells upon adhesion process, characterization of the morphological structure under the cell culture condition should be conducted [15].

Fundamental understanding of the phase separation and crystallization process in polymer blend and the key factors determining the patterning (microstructure and surface roughness) need to be examined in molecular level.

# CHAPTER 3

# RESULTS AND DISCUSSIONS FOR REGULATION OF CELLULAR FUNCTIONS BY CELL-TO-SURFACE INTERACTION

## 3.1. Response of culture cells grown on patterned biomaterial combinatorial library

It is desired to demonstrate cellular responses to libraries containing thousands of distinct surface properties. Earlier studies have shown that cells grown on uniformly patterned biomaterials give out distinct responses for each varied pattern [1, 9, 12, 23, 61].

In our result, we expect to observe a gradual change in the attachment density and cellular shape upon cellular interaction between osteoblast cells and biomaterial libraries of distinct chemistries, microstructures, and roughnesses. To serve those purposes, assays for cellular shape, size, and density were performed at 1 d of culture for MC3T3-E1 cells. The results are presented in the following sections.

### 3.1.1. Attachment density

Attachment density was measured by counting cell populations whose nuclei were stained with Hoechst (blue).

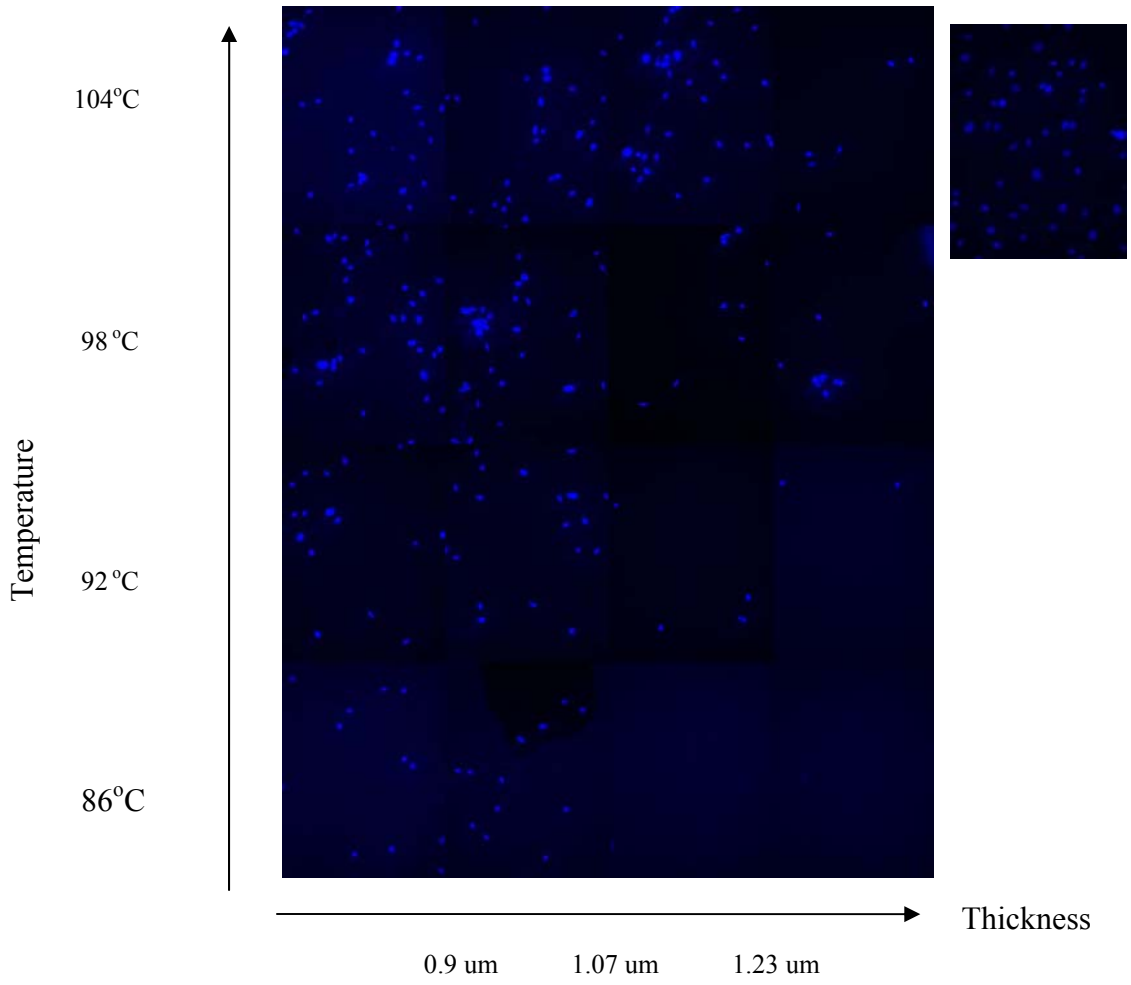


Figure 26. Fluorescence Image of 16 points from combinatorial sample, showing gradual change of density along T and h gradient. Each image is 433.33 x 325 μm in size. Insert: positive control on PS dish.

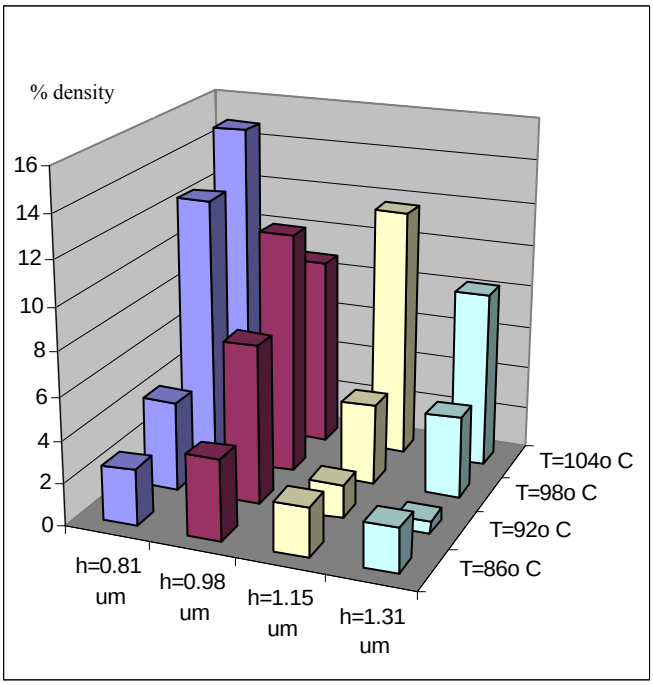


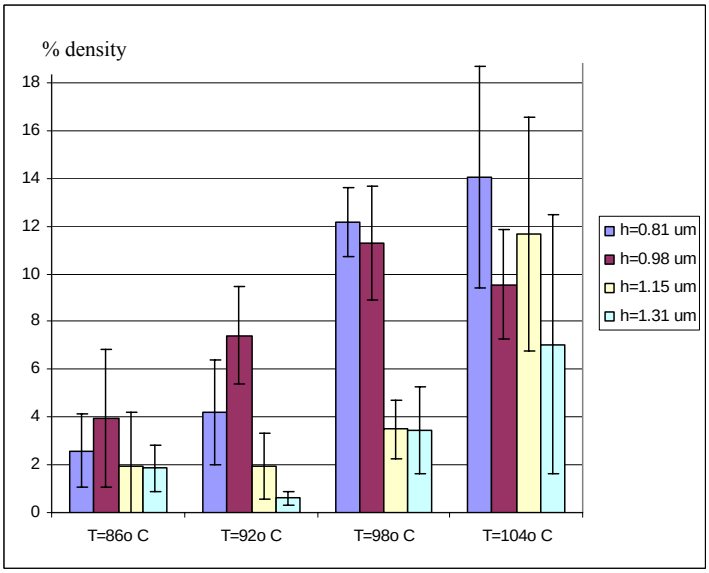


Figure 27. Cell attachment density from cells cultured on combinatorial chip corresponding to Figure 14[14].

[14] Presented as percentage of population in each point over total population on the library. All points are significantly different from at least one other point at 95% confidence interval except point 2, 6, 8 and 16.

General trend shows higher attachment density (Figure 27) and larger cell area (Figure 30) of cell cultured on regions with lower film thickness and annealed with higher temperature. This region corresponds to the upper triangular half of Figure 14.

### 3.1.2. Cell shape and size

Cell shape can be inferred from actin protein staining (Rhodamine-Phalloidine, red).

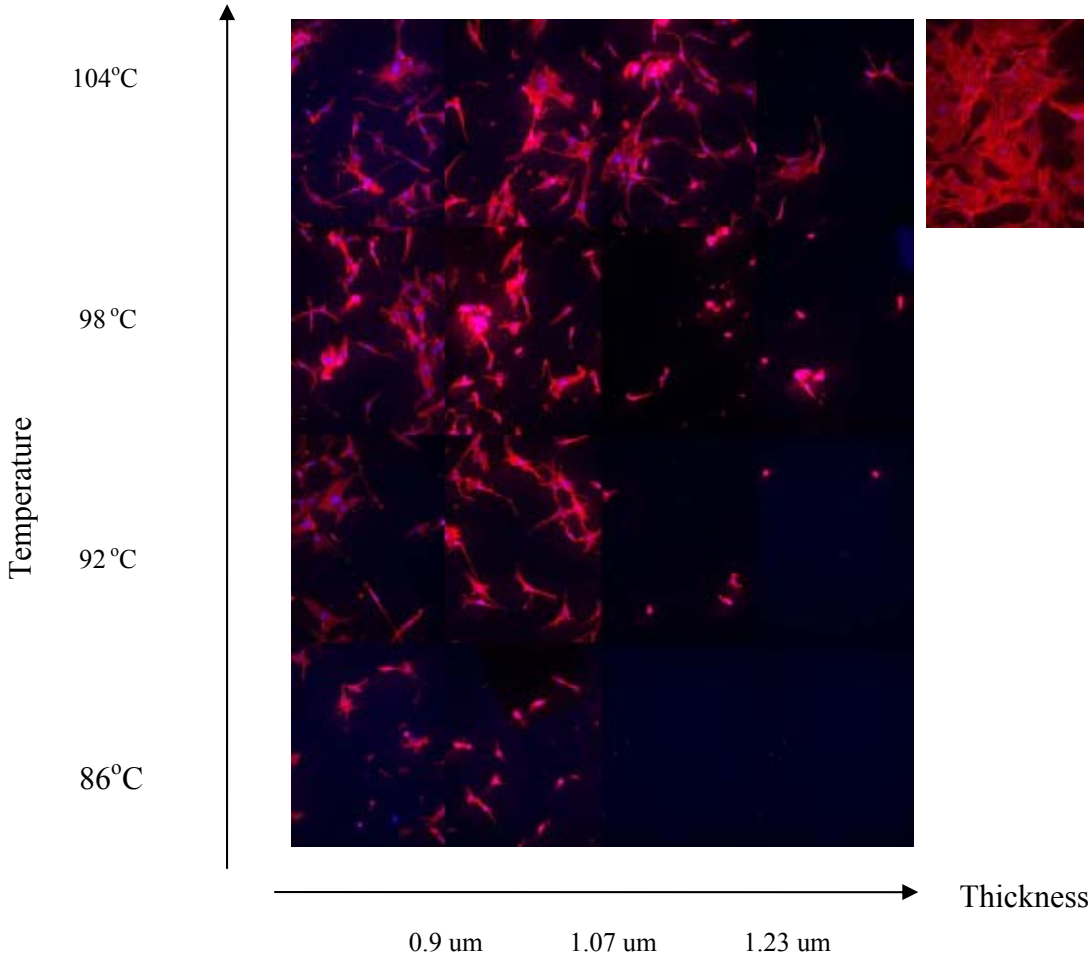


Figure 28. Fluorescence Image of 16 points from combinatorial sample, showing gradual change of cell size and shape along T and h gradient. Each image is 433.33 x 325 μm in size. Insert: positive control on PS dish.

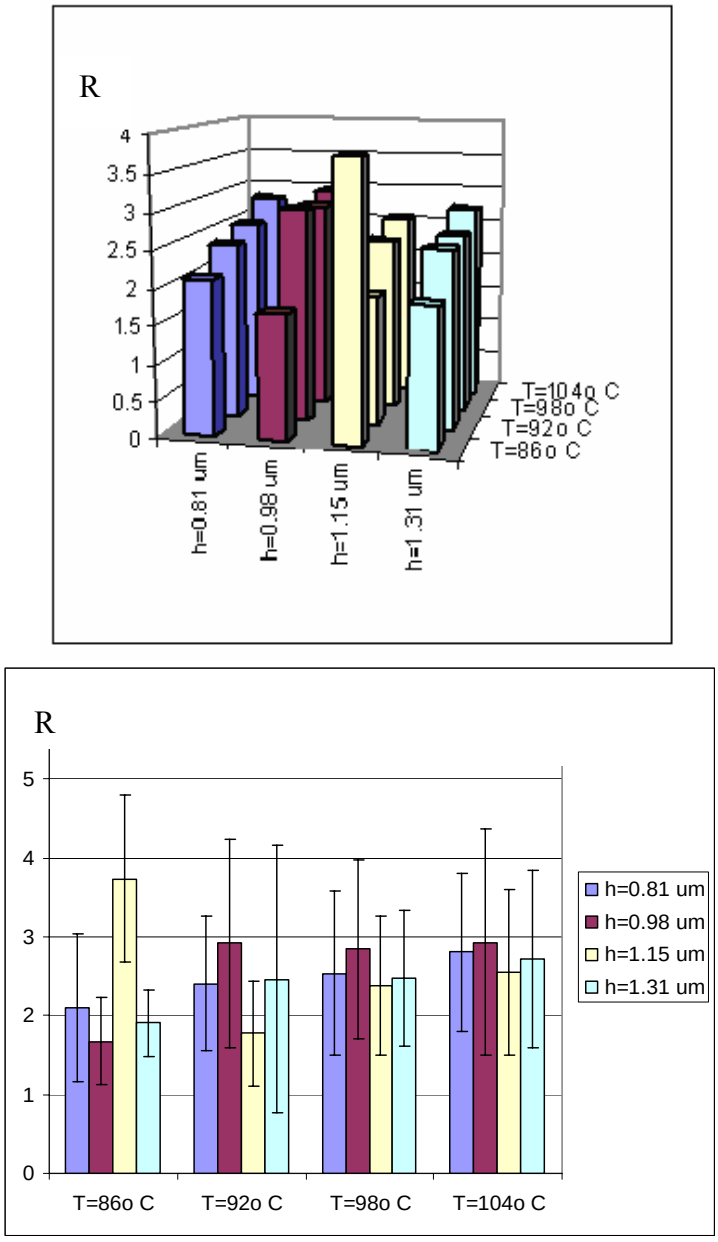


Figure 29. Cell roundness (R) from cells cultured on combinatorial chip corresponding to Figure 14[15].

[15] **Roundness (R)** is defined as $\text{Roundness} = \frac{\text{perimeter}^2}{4\pi.\text{area}}$. No point is significantly different from any other point at 95% confidence interval.

Cell roundness definition as described on page 59 dictates that perfectly circular cells will have a roundness value of 1, while any other shape will have value higher than 1. From the result presented in Figure 29, we can not draw any conclusion within 95% confidence range about the difference of cellular shape throughout the culture on combinatorial samples.

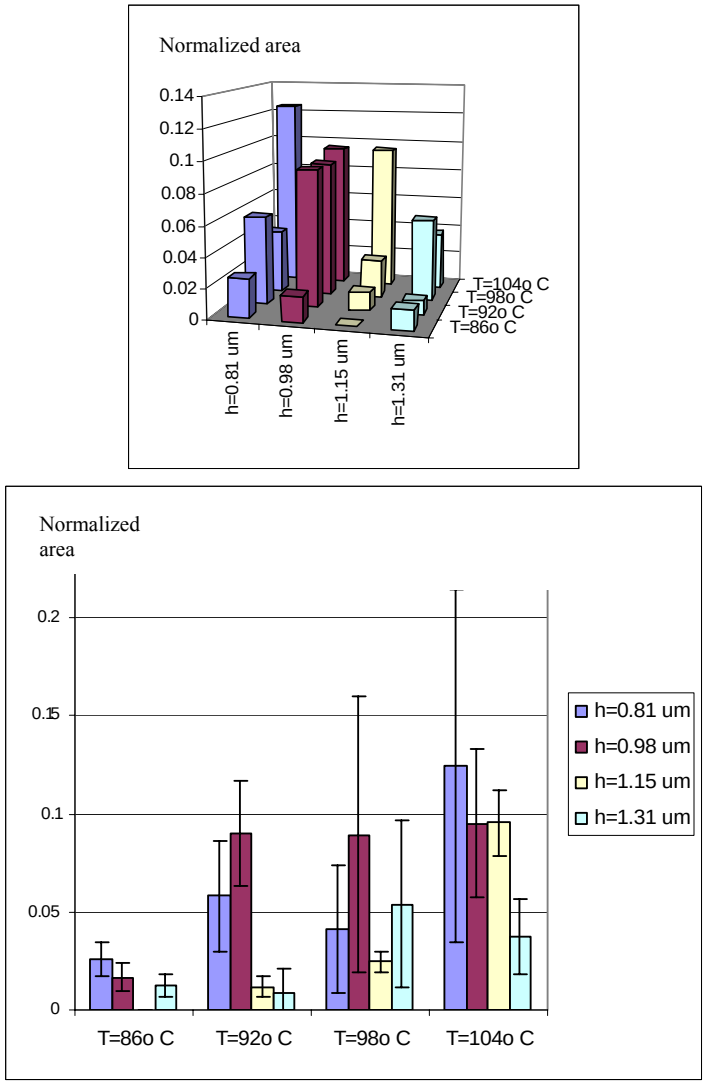


Figure 30. Cell area from cell cultured on combinatorial chip corresponding to Figure 13[16].

[16] Each value represented above is the value normalized to the weighted average value throughout each set of scan. Weighted average is computed based on attachment density data. No point is significantly different from any other point at 95% confidence interval.

3.1.3. Fibronectin adsorption

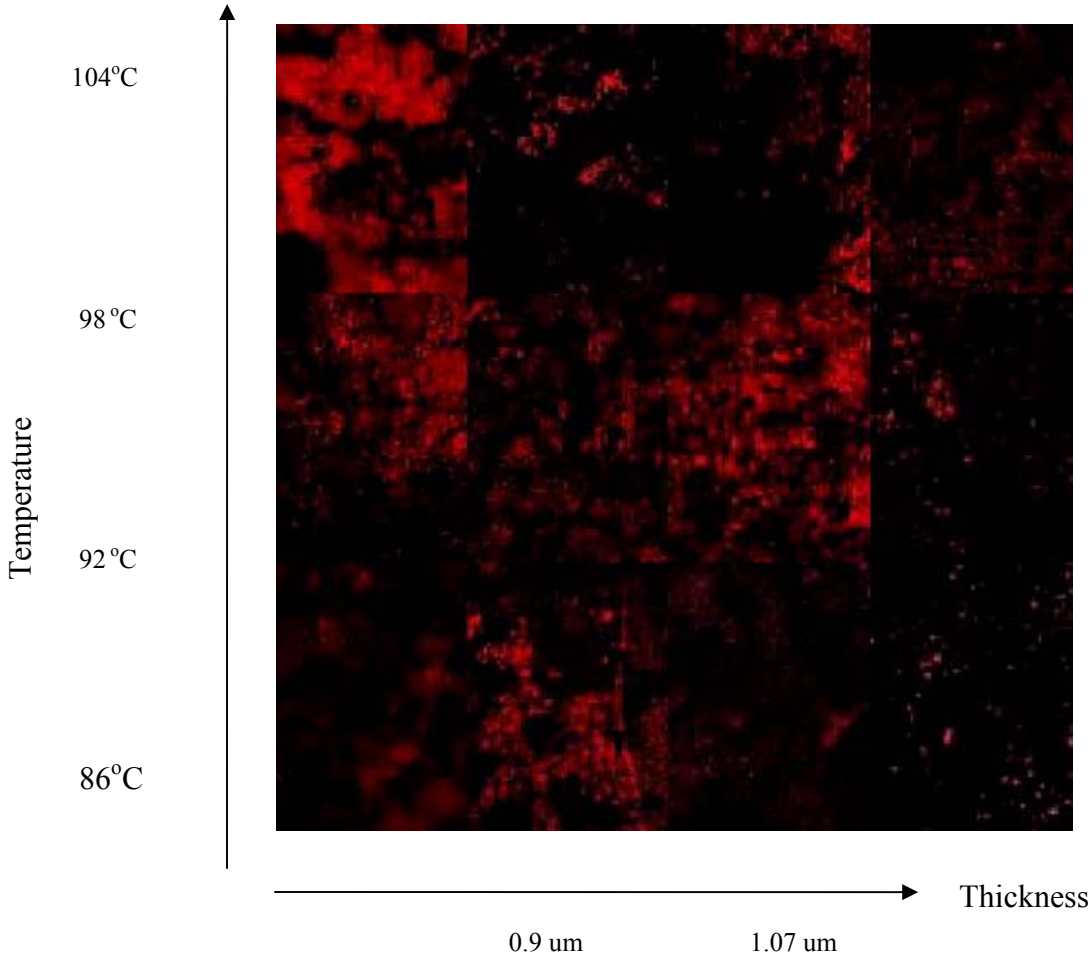


Figure 31. Fibronectin adsorption on the surface. Each image is 433.33 x 325 μm in size. Assay is done with Human Fibronectin stained with immunostaining method. The primary antibody is monoclonal (Rabbit) anti-human Fibronectin. The secondary antibody is polyclonal (Goat) anti-rabbit, tagged with red fluorofore functional group.

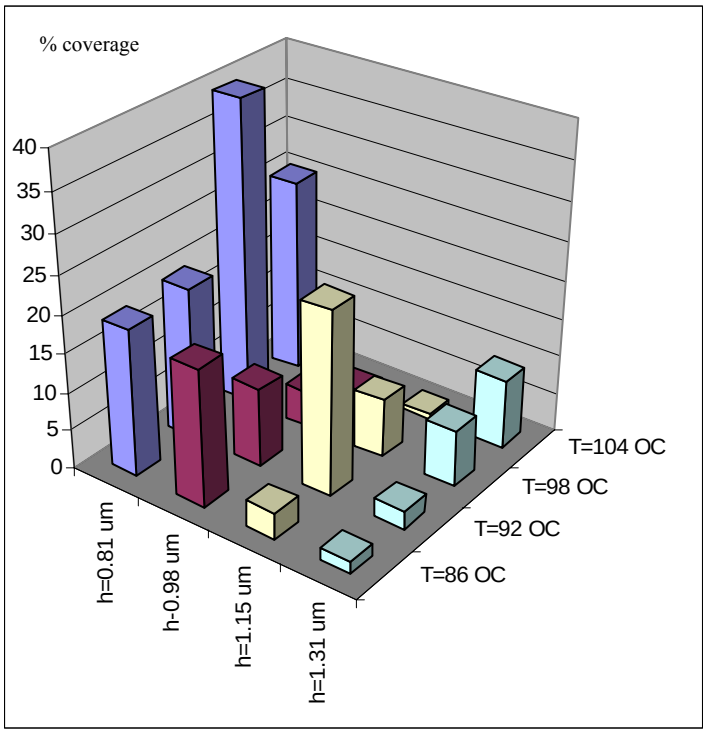


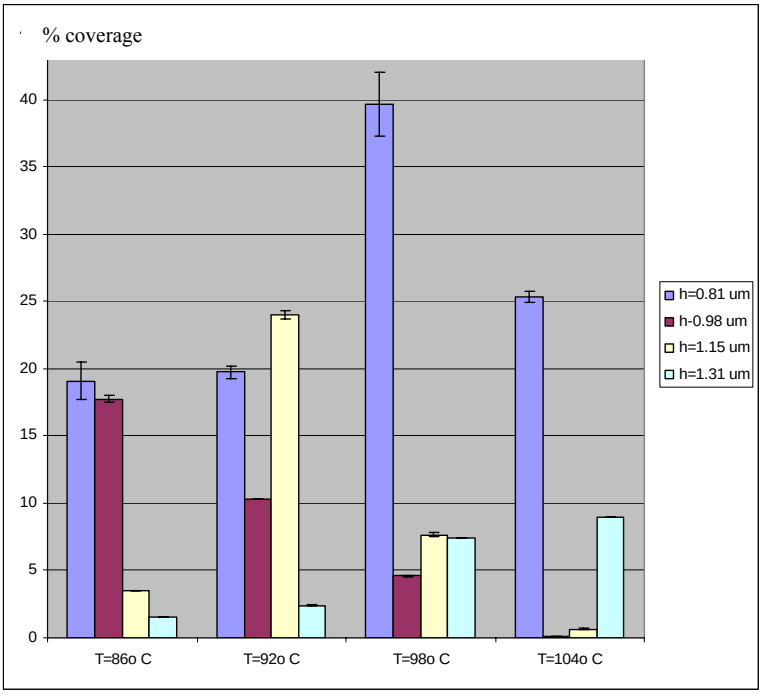


Figure 32. Fibronectin adsorption % coverage.

Fibronectin shows higher adsorption at the boundary of the two triangular halves corresponding to Figure 14. There was an exceptionally high Fibronectin adsorption on the lowest thickness region. This result showed different trend than what was expected before. Considering the previous trend of higher cellular attachment density and better spreading of the cells (indicated by larger cell area) at the upper triangular half, it was expected that Fn will have a higher adsorption at that particular region. The mismatch at 6,7,8, and 12 in Figure 32 (numbering refers to Figure 14) might be an effect of improper tagging, related to the folding of Fibronectin. This needs to be studied into more detail in the future research plan.

## 3.2. Correlation of cellular responses and biomaterial surface properties

### 3.2.1. General Observation

#### 3.2.1.1. Cell attachment density, cell shape, and cell size

From the result we can see that cellular size (Figure 30), and population density (Figure 27) response show similar and predictable trends with respect to the gradient of surface properties on the combinatorial libraries. The *general trend* is that higher values of cell attachment density and cell area were observed at higher annealing temperature and lower thickness. This is highly correlated to the same trend in microstructure and PCL-rich sub domain surface roughness. Larger and rougher areas of PCL-rich sub domain in the microstructure are located at higher annealing temperatures and on thinner film regions. Cellular sensitivity to PCL-related properties demonstrated the importance of the adhesive sub-domain patterning to cellular functions. This result is in accordance with those of previous studies[1-5, 9, 11, 12, 62, 63].

Optimum point with significantly higher cell attachment density and cell area coincided with medium to high microstructure and roughness. This can be observed by comparing the optimum area from Figure 27 and Figure 29 to the values shown in Figure 15 and Figure 22 at similar positions. Microstructure, represented by average area of PCL-rich sub domain, ranges from 20 to 50 $\mu m^2$; while PCL sub-domain surface roughness ranges from 60 to 80 nm for that optimum region.

Recent studies from Pedro Zapata, et al[17] showed similar trends in cellular attachment density and proliferation rate. In blend of PDLA-PCL, MCT3T3-E1 cells were shown to have higher proliferation at moderate T and $\varphi_{PCL}$, which corresponds to medium to high surface roughness. The range of optimum points is from 100 to 250 nm overall surface roughness.

Quantitatively, cellular shape showed no difference within 95% confidence in everywhere across the gradient in the library (also see Appendix A and B). The problem lies in the large degree of deviation from sample to sample. The general trend in cellular response was well-preserved from sample to sample; but was of different magnitude on each surface. This caused the standard deviation for each point in the averaged value in the library to be very large. This problem was amplified for the cell roundness observation due to the small detectable range of values for roundness parameter.

To illustrate this problem, we can examine the data for cell shape and size. The variance made it difficult to draw any conclusion. We can not justify that the gradual change of shape and size from point to point in the library because all points are not significantly different form the other points within 95% confidence interval. But we can still observe general trend in cell shape and size. Cells with rounder shape and larger

[17] Presented at Biomaterial Society Annual Symposium, Savannah, GA, 2003

surface area were located at the area where the values of microstructure and surface roughness are medium to high.

The problem with standard deviation values from cell size and shape data originated from the nature of data itself. Cellular shape and area vary in a much wider range compared to cellular count. Cell size and shape are highly fluctuating within each data sampling (image). This results in a lower degree of significance in point-to-point difference in their gradient values when compared to the significance of cellular density gradient.

#### 3.2.1.2. Fibronectin adsorption

Result shows qualitatively that Fibronectin did not adsorb strongly on totally amorphous or highly crystalline surfaces. This can be observed from comparing Figure 14 to Figure 32. Fibronectin adsorption shown in Figure 32 was significantly higher in the *boundary area* of hazy triangular half and transparent triangular half of the sample corresponding to Figure 14. This may be caused by the difference in surface roughness (physical property) at sub domain level, the difference in adhesiveness (chemistry), or the interplay between the former two factors.

Surface properties may be correlated to cellular response as shown in sub chapters 3.2.1.1 and 3.2.1.2 through Fibronectin adsorption result. The rationale behind cell adhesion's dependency on surface roughness and microstructure will be presented in the following sub chapters.

### 3.2.2. Correlation of chemistry to cellular adhesion

The results from cellular response mentioned earlier in 3.2.1 can be linked to surface properties libraries presented in 2.3 through the chemistry of the surface. Adhesive PCL sub-domain has preferentially adsorb protein. Fibronectin is known to be one of the crucial adhesion proteins for osteoblast [1, 9, 12, 15, 23, 34, 35].

Cellular responses can be correlated to surface properties through ECM protein adsorption. In this research, Fibronectin is chosen for the assay of adhesion protein. It has been shown that there is an critical value for Fibronectin concentration related to cell adhesion [64].

Result shows that Fibronectin had a preferential adsorption on the *boundary area* of low-crystallinity contrast (opaque part) and high-crystallinity contrast (transparent part) of the two triangular halves in the microstructure library (compare Figure 14 to Figure 31 and Figure 32). At the same chemical content and microstructure size, different crystallinity and different contrast is "sensed" by the adhering protein, and this sensing is transmitted to cellular response through cellular signaling pathways activated after cellular attachment. This is in line with the results from previous studies [1, 9, 12, 15, 23, 34, 35].

### 3.2.3. Correlation of surface physical properties to cellular adhesion

Other than adhesiveness contrast, sub domain surface roughness might also contribute to Fibronection adsorption. The size of Fibronectin is 170 kDa, approximately 80 nm [65], and is within the same order of magnitude as the surface roughness of the boundary region of the two triangular halves corresponding to Figure 14. The surface roughness value in this region is in the order of 100 nm. Previous investigations of the

functionality and folding of the protein on are proven to be determining on cellular adhesion [11, 12]. With incorrect folding, Fibronectin does not have a strong adhesion or activity on the surface.

From the microstructure features, the cell actually prefers a certain spacing of the adhesive versus non-adhesive pattern. Similar preferences have been observed previously for patterned surface with Fibronectin coating on the micro structural features [9]. This information can be inferred qualitatively from Figure 14 and the results presented in this chapter. Quantitative analysis for microstructure spacing, in additional to sub domains' area ratio, is needed for further improvement.

### 3.3. Conclusion

From the results and background above, we begin to rationalize the dependency of cell adhesion on surface roughness and microstructure. In addition, these results are useful for designing new experiments.

The trend of cellular responses to regions of biomaterial surface libraries was demonstrated consistently in all points of interest. Generally, higher values for cell roundness, cell attachment density, and cell area are located at higher T and lower thickness. This corresponds to largest microstructure size (20 to 50 $\mu m^2$) and surface roughnesses (100 to 180 nm) presented in Chapter 2. Also these physical properties were located in regions with highest crystallinity contrast. Therefore, the result demonstrated the correlation of cellular response upon adhesion to surface properties.

### 3.4. Future Improvement Plan

Dependence of cell response on microstructural spacing is still left unexplored in this result. Quantitative data analysis for microstructure and cellular spacing is needed to get a better correlation between the two.

Distribution of the surface properties within each point may also play an important role in determining cellular responses. This aspect should be inter-related to the degree of contrast in the properties of two distinct sub domains.

Previous studies have shown the correlation of cell shape to cellular functions [1, 9, 12, 15, 23, 34, 35]. Therefore, further assays on those biological functions such as proliferation, apoptosis, and protein expressions should be examined into more details.

For future reference, quantitative measurement of crystallinity needs to be performed to correlate it to adhesiveness and cellular adhesion.

In addition to time and resource constraints for biological assays, the need of a large number of data in the library is a critical issue as demonstrated in this research thesis. This is caused by the statistical nature of cellular response. Larger amount of data is needed to improve confidence interval of the trend observed.

Data mining method should be incorporated and improved to accommodate the need of large amount of data and to sensitively recognize patterns in the library.

# CHAPTER 4

# CONCLUSION AND FUTURE IMPROVEMENT PLAN

## 4.1. Conclusion

Combinatorial techniques utilizing phase separation and difference in crystallization rate is shown to create successfully libraries with diverse microstructure and surface roughness.

The contrast provided in the library encompasses variations in adhesive and non-adhesive sub domains and surface roughness.

Bigger microstructure (20 to 50 $\mu m^2$) and rougher surface (100 to 180 nm) were achieved at higher T and lower film thickness. Sharp boundary at transition points where crystallinity contrast was large showed better physical properties

The trend of cellular response to surface properties library was consistently demonstrated in all points of interest. Optimum surface properties for cellular attachment density, cellular shape and size were achieved with surface prepared at medium to high microstructure (20 to 50 $\mu m^2$) and surface roughness (100 to 180 nm).

## 4.2. Future Improvement Plan

Additional data sets required for future reference are:

1. Mechanical properties of the biomaterial and the correlation of this particular property to cellular behaviors.
2. Microstructure spacing is still left unexplored in this result. Quantitative analysis is needed to have a better description of surface properties library.

3. Real-time morphological structure characterization under the cell culture condition should be conducted.
4. Fundamental understanding of the phase separation and crystallization process in polymer blend and the key factors determining the patterning (microstructure and surface roughness) need to be examined in molecular level.
5. Distribution, in addition to the mean value, of the surface properties within each point may also play an important role in determining cellular responses. This aspect should be inter-related to the degree of contrast in the properties of two distinct sub domains.
6. Quantitative measurement of crystallinity needs to be performed to correlate it to adhesiveness and cellular adhesion.
7. Correlation of cellular functions to cellular shape and area, and to surface properties.
8. Larger number of data in the library is a critical issue to improve confidence interval of the trend observed as demonstrated in this research thesis. This is caused by the statistical nature of cellular response. Data mining method should be incorporated and improved to accommodate the need of large amount of data and to sensitively recognize patterns in the library.
9. Checking of chemical presentation on the surface. From results in bilayer, it might be inferred that PCL is the overlayer, but cells are not responding well.

10. Improvement on range of surface properties, to make sure we find optimum value, not just maximum value within one sample.

## APPENDIX A

## SAMPLE OF STATISTICAL ANALYSIS

An example is shown for microstructure. Data sampling is performed by taking 3 different samples. Three data points are taken for each position in each sample[18].

Table 6. Microstructure size (in pixels) for each position in the sample.

| Position | Sample #3 | Sample #4 | Sample #9 | Average | Std. Dev. |
|---|---|---|---|---|---|
| 1 | 4.4153 | 4.32938 | 4.3 | 4.372335 | 0.060749 |
| 2 | 2.5465 | 3.76067 | 3.15 | 3.153589 | 0.858541 |
| 3 | 4.7972 | 5.4975 | 3.65135 | 4.648677 | 0.931989 |
| 4 | 7.1614 | 6.77317 | 9.31682 | 7.750458 | 1.370327 |
| 5 | 2.7329 | 5.0146 | 3.87 | 3.873726 | 1.61344 |
| 6 | 5.2309 | 3.427 | 4.32 | 4.328953 | 1.275557 |
| 7 | 4.838 | 6.02028 | 5.42 | 5.429152 | 0.835974 |
| 8 | 3.7989 | 6.9868 | 8.15018 | 6.311946 | 2.252794 |
| 9 | 3.1986 | 3.44941 | 3.32 | 3.323981 | 0.177377 |
| 10 | 2.812 | 3.96633 | 3.28 | 3.389186 | 0.816208 |
| 11 | 3.3219 | 4.58963 | 3.95 | 3.95575 | 0.896444 |
| 12 | 3.7758 | 3.97827 | 3.88 | 3.877016 | 0.143192 |
| 13 | 5.1905 | 3.39049 | 4.3 | 4.290482 | 1.272786 |
| 14 | 4.1066 | 4.19119 | 4.14 | 4.148878 | 0.059833 |
| 15 | 7.9889 | 3.43873 | 5.71 | 5.713794 | 3.217423 |
| 16 | 7.9839 | 8.16353 | 8.1 | 8.07369 | 0.127051 |

[18] Except for roughness data, only one data point is retrieved from each position in each sample.

Table 7. Sample calculation result for ANOVA1 Statistical analysis performed with Matlab ® for Microstructure data at position 1 in the library[19].

ANOVA Table

| Source | SS | df | MS | F | Prob>F |
|---|---|---|---|---|---|
| Columns | 0.784 | 2 | 0.39176 | 0.13 | 0.8776 |
| Error | 134.678 | 45 | 2.99285 | | |
| Total | 135.462 | 47 | | | |

The result shows that sample #3, #4, and #9 are not significantly different from one and another ($p<0.05$). This means the experimental design and result are repeatable

Table 8. Sample calculation for ANOVA2 Statistical analysis performed with Matlab ® for microstructure corresponding to Table 6.

ANOVA Table

| Source | SS | df | MS | F | Prob>F |
|---|---|---|---|---|---|
| Columns | 24.188 | 3 | 8.0625 | 7.41 | 0.0007 |
| Rows | 56.982 | 3 | 18.9939 | 17.45 | 0 |
| Interaction | 19.455 | 9 | 2.1616 | 1.99 | 0.0745 |
| Error | 34.838 | 32 | 1.0887 | | |
| Total | 135.462 | 47 | | | |

The result shows that both annealing temperature (T) and thickness (h) gradients affect microstructure significantly from point to point. Both p values for each factor are less than 0.05. Furthermore, the interaction between T and h is not significant ($p>0.05$)

[19] Data not shown

Multivariable statistical analysis is performed to check certain points within samples that is significantly different from the rest.

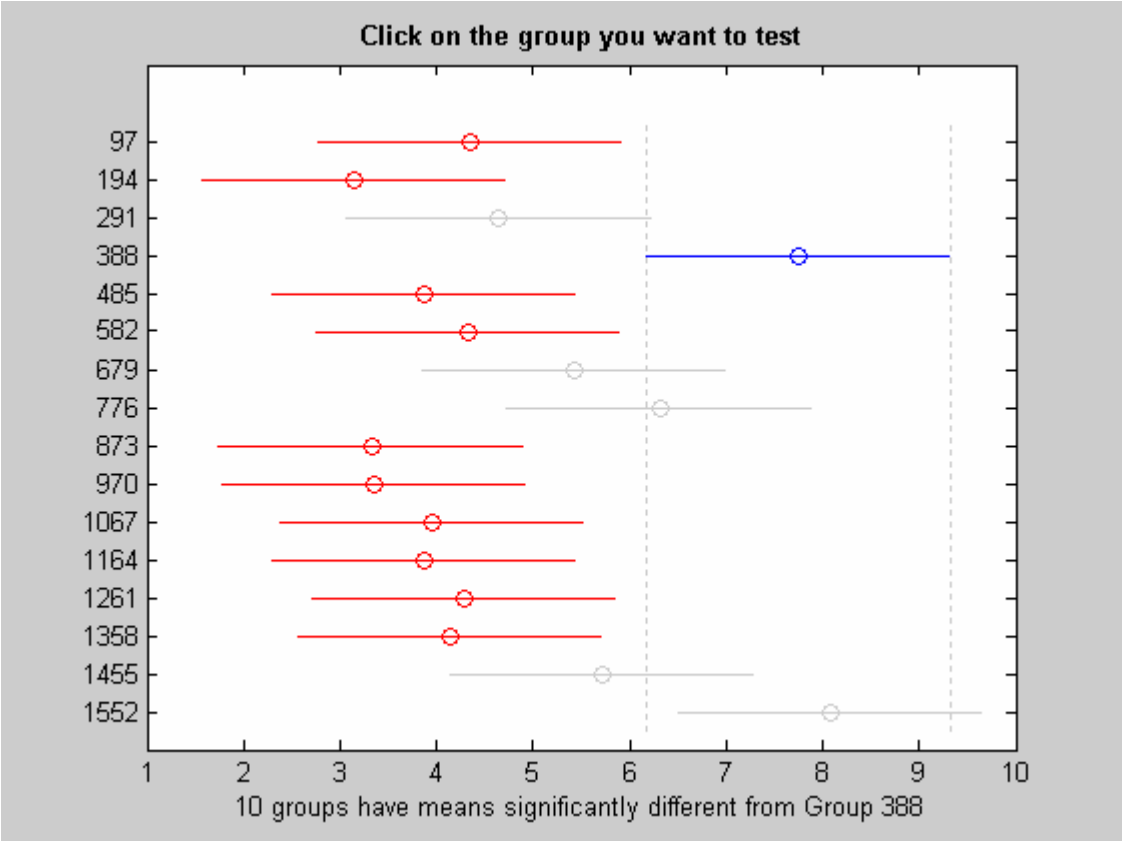


Figure 33. Sample of multivariable comparison. Comparison is done on all possible pairings between 16 points in the full scanned sample.

The system for numbering follows ASCII code that starts with 97 for 'a'. Number 97 corresponds to point 1. From point 2 onward, numbering follows similar fashion. Result shows that point 8 is significantly different from one other point; point 4 from 10 other points, while point 16 from 11 other points. In Figure 33, result is shown for comparison of point 4 to all other points. Red margin signifies significant difference with other point.

The summary of Matlab ® functions used for statistical analysis is described below.

*1. anova1*

A balanced one-way ANOVA for comparing the means of two or more columns of data in the m-by-n matrix X, where each column represents an independent sample containing m mutually independent observations. The function returns the p-value for the null hypothesis that all samples in X are drawn from the same population (or from different populations with the same mean).

The *anova1* test evaluates the hypothesis that the samples all have the same mean against the alternative that the means are not all the same. This test is used to **check the consistency of data** from each sample and observation for each position of interest in the scanning of a particular surface property or cellular response. If $p<0.05$ then all samples are significantly different from one and another within 95% confidence. *Anova1* was applied to 3 sets of data. Each set is the data set obtained from each samples. Columns correspond to samples, rows corresponds to the repetition in the data sampling from each sample. Therefore, *anova1* is performed for all the 16 positions for each set of library. The ideal result is that all data sets are consistent ($p>0.05$).

*2. anova2*

A balanced two-way ANOVA for comparing the means of two or more columns and two or more rows of the observations in X. The data in different columns represent changes in factor A. The data in different rows represent changes in factor B.

Replications in the data set represent the number of samples.

*Anova2* returns three p-values in vector p. They are:

1. the p-value for the null hypothesis, $H_{0A}$ (that all samples from factor A, i.e. all column-samples in X, are drawn from the same population)

2. the p-value for the null hypothesis, $H_{0B}$ (that all samples from factor B, i.e. all row-samples in X are drawn from the same population)
3. the p-value for the null hypothesis, $H_{0AB}$, that the effects due to factors A and B are additive (i.e., that there is no interaction between factors A and B).

The *anova2* test evaluates the hypothesis that the row, column, and interaction effects are all the same, against the alternative that they are not all the same. Sometimes it is preferable to perform a test to determine which pairs of effects are significantly different, and which are not. Use the multcompare function to perform such tests by supplying the stats structure as input.

The *anova2* test evaluates the hypothesis that the row, column, and interaction effects are all the same, against the alternative that they are not all the same. This test is used to **check the significance** of **gradual change** in the mean value calculated for each position in the library.

If $p_i<0.05$ then we can reject null hypothesis $H_{0i}$ within 95% confidence.

*Anova2* was applied to mean values in the library of each sample surface property or cellular response of interest.

*Anova2* is performed for each surface property or cellular response of interest.

The ideal result is that all data columns and rows are significantly different from one and another ($p<0.05$); i.e. there is a significant effect of the control variables (T and h) on the observed property in the library.

*3.* multcompare

*Multcompare* works on the statistical output from *anova1*. The output contains the results of the test in the form of a five-column matrix. Each row of the matrix represents one test, and there is one row for each pair of groups. The entries in the row indicate the means being compared, the estimated difference in means, and a confidence interval for the difference.

*Multcompare* performs a test on the mean value of each final library for each surface property or cellular response.

This is to check **which pairs of positions in the library** are significantly different, and which are not.

For example, suppose one row contains the following entries:

[2  5  1.9442  8.2206  14.4971].

These numbers indicate that the mean of group 2 minus the mean of group 5 is estimated to be 8.2206, and a 95% confidence interval for the true mean is [1.9442, 14.4971]. If the confidence interval contains 0.0, the difference would not be significant at the 0.05 level.

The ideal result is that each positions are significantly different from all other points ($p<0.05$).

## APPENDIX B

## SAMPLE OF STATISTICAL ANALYSIS RESULT

## FOR MULTI PAIRINGS COMPARISON

To interpret the results from *multcompare*, any point to point pairing that includes zero within the confidence range means they are not significantly different from each other. A sample of *multcompare* result is presented as follows.

Table 9. Result for PCL-rich sub domain surface roughness (all points have $p<0.05$).

| Point | Point | Min | Median | Max |
|---|---|---|---|---|
| 1 | 2 | -50.1541 | -26.764 | -3.374 |
| 1 | 3 | -49.5152 | -26.1251 | -2.735 |
| 1 | 4 | -152.103 | -128.713 | -105.323 |
| 1 | 5 | -25.237 | -1.8469 | 21.5431 |
| 1 | 6 | -151.572 | -128.182 | -104.792 |
| 1 | 7 | -21.1484 | 2.2416 | 25.6317 |
| 1 | 8 | -58.7718 | -35.3817 | -11.9917 |
| 1 | 9 | -16.1561 | 7.234 | 30.6241 |
| 1 | 10 | -55.9895 | -32.5994 | -9.2093 |
| 1 | 11 | -56.1615 | -32.7714 | -9.3813 |
| 1 | 12 | -73.085 | -49.6949 | -26.3049 |
| 1 | 13 | -30.2221 | -6.832 | 16.5581 |
| 1 | 14 | -55.2849 | -31.8949 | -8.5048 |
| 1 | 15 | -61.5772 | -38.1871 | -14.797 |
| 1 | 16 | -68.9514 | -45.5613 | -22.1713 |
| 2 | 3 | -22.7511 | 0.6389 | 24.029 |
| 2 | 4 | -125.339 | -101.949 | -78.559 |
| 2 | 5 | 1.527 | 24.9171 | 48.3072 |
| 2 | 6 | -124.808 | -101.418 | -78.0282 |
| 2 | 7 | 5.6156 | 29.0057 | 52.3958 |
| 2 | 8 | -32.0078 | -8.6177 | 14.7724 |
| 2 | 9 | 10.608 | 33.998 | 57.3881 |
| 2 | 10 | -29.2254 | -5.8353 | 17.5547 |
| 2 | 11 | -29.3974 | -6.0073 | 17.3827 |
| 2 | 12 | -46.321 | -22.9309 | 0.4592 |
| 2 | 13 | -3.458 | 19.9321 | 43.3221 |
| 2 | 14 | -28.5209 | -5.1308 | 18.2593 |
| 2 | 15 | -34.8131 | -11.4231 | 11.967 |

**Table 9** (continued)

| Point | Point | Min | Median | Max |
|---|---|---|---|---|
| 2 | 16 | -42.1874 | -18.7973 | 4.5928 |
| 3 | 4 | -125.978 | -102.588 | -79.1979 |
| 3 | 5 | 0.8881 | 24.2782 | 47.6682 |
| 3 | 6 | -125.447 | -102.057 | -78.6672 |
| 3 | 7 | 4.9767 | 28.3668 | 51.7568 |
| 3 | 8 | -32.6467 | -9.2566 | 14.1334 |
| 3 | 9 | 9.969 | 33.3591 | 56.7492 |
| 3 | 10 | -29.8644 | -6.4743 | 16.9158 |
| 3 | 11 | -30.0364 | -6.6463 | 16.7438 |
| 3 | 12 | -46.9599 | -23.5698 | -0.1798 |
| 3 | 13 | -4.097 | 19.2931 | 42.6832 |
| 3 | 14 | -29.1598 | -5.7698 | 17.6203 |
| 3 | 15 | -35.4521 | -12.062 | 11.3281 |
| 3 | 16 | -42.8263 | -19.4362 | 3.9538 |
| 4 | 5 | 103.4761 | 126.8661 | 150.2562 |
| 4 | 6 | -22.8593 | 0.5307 | 23.9208 |
| 4 | 7 | 107.5647 | 130.9547 | 154.3448 |
| 4 | 8 | 69.9413 | 93.3313 | 116.7214 |
| 4 | 9 | 112.557 | 135.9471 | 159.3372 |
| 4 | 10 | 72.7236 | 96.1137 | 119.5038 |
| 4 | 11 | 72.5516 | 95.9417 | 119.3318 |
| 4 | 12 | 55.6281 | 79.0181 | 102.4082 |
| 4 | 13 | 98.491 | 121.8811 | 145.2712 |
| 4 | 14 | 73.4282 | 96.8182 | 120.2083 |
| 4 | 15 | 67.1359 | 90.526 | 113.9161 |
| 4 | 16 | 59.7617 | 83.1517 | 106.5418 |
| 5 | 6 | -149.726 | -126.335 | -102.945 |
| 5 | 7 | -19.3015 | 4.0886 | 27.4787 |
| 5 | 8 | -56.9249 | -33.5348 | -10.1447 |
| 5 | 9 | -14.3091 | 9.0809 | 32.471 |
| 5 | 10 | -54.1425 | -30.7524 | -7.3624 |
| 5 | 11 | -54.3145 | -30.9244 | -7.5344 |
| 5 | 12 | -71.2381 | -47.848 | -24.4579 |
| 5 | 13 | -28.3751 | -4.9851 | 18.405 |
| 5 | 14 | -53.438 | -30.0479 | -6.6578 |
| 5 | 15 | -59.7302 | -36.3402 | -12.9501 |
| 5 | 16 | -67.1045 | -43.7144 | -20.3243 |
| 6 | 7 | 107.0339 | 130.424 | 153.8141 |
| 6 | 8 | 69.4105 | 92.8006 | 116.1907 |
| 6 | 9 | 112.0263 | 135.4163 | 158.8064 |
| 6 | 10 | 72.1929 | 95.583 | 118.973 |
| 6 | 11 | 72.0209 | 95.411 | 118.801 |
| 6 | 12 | 55.0973 | 78.4874 | 101.8775 |
| 6 | 13 | 97.9603 | 121.3504 | 144.7404 |

**Table 9** (continued)

| Point | Point | Min | Median | Max |
|---|---|---|---|---|
| 6 | 15 | 66.6052 | 89.9952 | 113.3853 |
| 6 | 16 | 59.2309 | 82.621 | 106.0111 |
| 7 | 8 | -61.0135 | -37.6234 | -14.2333 |
| 7 | 9 | -18.3977 | 4.9924 | 28.3824 |
| 7 | 10 | -58.2311 | -34.841 | -11.451 |
| 7 | 11 | -58.4031 | -35.013 | -11.623 |
| 7 | 12 | -75.3267 | -51.9366 | -28.5465 |
| 7 | 13 | -32.4637 | -9.0736 | 14.3164 |
| 7 | 14 | -57.5266 | -34.1365 | -10.7464 |
| 7 | 15 | -63.8188 | -40.4288 | -17.0387 |
| 7 | 16 | -71.1931 | -47.803 | -24.4129 |
| 8 | 9 | 19.2257 | 42.6157 | 66.0058 |
| 8 | 10 | -20.6077 | 2.7824 | 26.1724 |
| 8 | 11 | -20.7797 | 2.6104 | 26.0004 |
| 8 | 12 | -37.7033 | -14.3132 | 9.0769 |
| 8 | 13 | 5.1597 | 28.5498 | 51.9398 |
| 8 | 14 | -19.9032 | 3.4869 | 26.877 |
| 8 | 15 | -26.1954 | -2.8054 | 20.5847 |
| 8 | 16 | -33.5697 | -10.1796 | 13.2105 |
| 9 | 10 | -63.2235 | -39.8334 | -16.4433 |
| 9 | 11 | -63.3955 | -40.0054 | -16.6153 |
| 9 | 12 | -80.319 | -56.9289 | -33.5389 |
| 9 | 13 | -37.4561 | -14.066 | 9.3241 |
| 9 | 14 | -62.5189 | -39.1289 | -15.7388 |
| 9 | 15 | -68.8112 | -45.4211 | -22.031 |
| 9 | 16 | -76.1854 | -52.7953 | -29.4053 |
| 10 | 11 | -23.5621 | -0.172 | 23.2181 |
| 10 | 12 | -40.4856 | -17.0956 | 6.2945 |
| 10 | 13 | 2.3773 | 25.7674 | 49.1575 |
| 10 | 14 | -22.6855 | 0.7045 | 24.0946 |
| 10 | 15 | -28.9778 | -5.5877 | 17.8024 |
| 10 | 16 | -36.352 | -12.962 | 10.4281 |
| 11 | 12 | -40.3136 | -16.9236 | 6.4665 |
| 11 | 13 | 2.5493 | 25.9394 | 49.3295 |
| 11 | 14 | -22.5135 | 0.8765 | 24.2666 |
| 11 | 15 | -28.8058 | -5.4157 | 17.9744 |
| 11 | 16 | -36.18 | -12.79 | 10.6001 |
| 12 | 13 | 19.4729 | 42.8629 | 66.253 |
| 12 | 14 | -5.59 | 17.8001 | 41.1902 |
| 12 | 15 | -11.8822 | 11.5078 | 34.8979 |
| 12 | 16 | -19.2565 | 4.1336 | 27.5237 |
| 13 | 14 | -48.4529 | -25.0629 | -1.6728 |
| 13 | 15 | -54.7452 | -31.3551 | -7.965 |

**Table 9** (continued)

| Point | Point | Min | Median | Max |
|---|---|---|---|---|
| 13 | 16 | -62.1194 | -38.7293 | -15.3393 |
| 14 | 15 | -29.6823 | -6.2922 | 17.0978 |
| 14 | 16 | -37.0566 | -13.6665 | 9.7236 |
| 15 | 16 | -30.7643 | -7.3742 | 16.0158 |

## REFERENCES


1. Meredith, J.C., et al., *Combinatorial characterization of cell interactions with polymer surfaces.* J Biomed Mater Res, 2003. **66A**(3): p. 483-90.
2. Brocchini, S., K. James, V. Tangpasuthadol, and J. Kohn, *A combinatorial approach for polymer design.* J. Amer. Chem. Soc., 1997. **119**(19): p. 4553-4554.
3. Brocchini, S., et al., *Structure-property correlations in a combinatorial library of degradable biomaterials.* J Biomed Mater Res, 1998. **42**(1): p. 66-75.
4. B. J. Spargo, e.a., *Spatially controlled adhesion, spreading, and differentiation of endothelial cells on self-assembled molecular monolayer.* Proc. Nat. Acad. Sci, 1994. **91**: p. 11070-11074.
5. C. S. Ranucci, P.V.M., *Polymer Substrate topography actively regulates the multicellular organization and liver-specific functions of cultured hepatocytes.* Tissue Eng., 1999. **5**: p. 407-420.
6. Evangelos Tziampazis, J.K., Prabhas V. Moghe, *PEG-variant biomaterials as selectively adhesive protein templates: model surfaces for controlled cell adhesion and migration.* Biomaterials, 2000. **21**: p. 511-520.
7. Ratner BD, C.D., Horbett TA, Lenk TJ, Lewis KB, Rapoza RJ, *Biomolecular and Surfaces.* Vac. Sci. Technol. A., 1990. **8**(3): p. 2306-2317.
8. Sarikaya, M., et al., *Molecular biomimetics: nanotechnology through biology.* Nat Mater, 2003. **2**(9): p. 577-85.
9. Christopher S. Chen, e.a., *Geometric control of cell life and death.* Science, 1997. **276**(5317): p. 1425-1428.
10. Chen, G., Y. Imanishi, and Y. Ito, *Effect of protein and cell behavior on pattern-grafted thermoresponsive polymer.* J Biomed Mater Res, 1998. **42**(1): p. 38-44.
11. A. Garcia, P.D., D. Boettiger, *The effect of surface reaction stage on fibronectin-mediated adhesion of osteoblast-like cells to bioactive glass.* J. Biomed. Mater. Res., 1998. **40**: p. 48-56.
12. A. Garcia, P.D., D. Boettiger, *Modulation of cell proliferation and differentiation trhough substrate-dependent changes in fibronectin conformation.* Mol. Biol. Cell, 1999. **10**: p. 785-798.
13. Braun, R., M. Sarikaya, and K. Schulten, *Genetically engineered gold-binding polypeptides: structure prediction and molecular dynamics.* J Biomater Sci Polym Ed, 2002. **13**(7): p. 747-57.
14. Bruggemann, O., *Molecularly imprinted materials--receptors more durable than nature can provide.* Adv Biochem Eng Biotechnol, 2002. **76**: p. 127-63.
15. S. Huang, D.I., *Shape-dependent control of cell growth, differentiation, and apoptosis: Switching between attactors in cell regulatory network.* Exp. Cell. Res., 2000. **261**: p. 91-103.
16. D. Itoh, S.Y., S. Kuroda, H. Kondo, A. Umezawa, K. Ohya, . Ohyama, S. Kasugai, *Enhancement of osteogenesis on hydroxyapatite surface coated with synthetic peptide (EEEEEEEPRGDT) in vitro.* 2002: p. 292-297.

17. D.H. Davis, C.S.G., R.W. Johnson, T.A. Desai, *Immobilization of RGD to <111> silicon surfaces for enhanced cell adhesion and proliferation.* Biomaterials, 2002. **23**: p. 4019-4027.
18. Kao, W.J., *Evaluation of protein-modulated macrophage behavior on biomaterials: designing biomimetic materials for cellular engineering.* Biomaterials, 1999. **20**: p. 2213-2221.
19. L. Kam, W.S., J. N. Turner, R. Bizios, *Selective adhesion of astrocytes to surfaces modified with immobilized peptides.* Biomaterials, 2002. **23**: p. 511-515.
20. M. C. Porte-Durrieu, C.L., F. Villars, F. Lefebvre, S. Dutoya, A. Guette, L. Bordenave, C. Baquey, *Development of RGD peptides grafted onto silica surfaces: XPS characterization and human endothelial cell interaction.* 1999: p. 368-375.
21. P. Banerjee, D.J.I., A.M. Mayes, L.G. Griffith, *Polymer latexes for cell-resistant and cell-interactive surfaces.* 2000.
22. S.P. Massia, J.S., *Immobilized RGD peptides on surface-grafted dextran promote biospecific cell attachment.* 2001: p. 390-399.
23. Chen CS, e.a., *Cell Shape provides global control of focal adhesion assembly.* Biochemical and Biophysical Research Communication, 2003. **307**: p. 355-361.
24. John l. Tan, J.T., Dana M. Pirone, Darren S. Gray, Kiran Bhadriraju, Christopher S. Chen, *Cells lying on a bed of microneedles: An approach to isolate mechanical force.* PNAS, 2003. **100**(4): p. 1484-1489.
25. Gray DS, T.J., Chen CS, *Repositioning of cells by mechanotaxis on surfaces with micropatterned Young's modulus.* Journal of Biomedical Material Research, 2003. **66A**: p. 605-614.
26. Y. W. Fan, F.Z.C., L.N.Chen, Y. Zhai, Q.Y. Xu, I-S. Lee, *Adhesion of neural cells on silicon wafer with nano-topographic surface.* Applied Surface Science, 2002. **2002**(187): p. 313-318.
27. Hirokaju Kaji, e.a., *Microelectrochemical Approach to Induce Local Cell Adhesion and Growth on Substrates.* 2004. **20**: p. 16-19.
28. B. D. Boyan, T.W.H., D. D. Dean, Z. Schwartz, *Role of material surfaces in regulating bone and cartilage cell response.* Biomaterials, 1996. **17**: p. 137-146.
29. E. Ostuni, C.S.C., D.E. Ingber, G.M. Whitesides, *Selective Deposition of Proteins and Cells in Arrays of Microwells.* Langmuir, 2001. **17**: p. 2828-2834.
30. Gray, D.S., J. Tien, and C.S. Chen, *Repositioning of cells by mechanotaxis on surfaces with micropatterned Young's modulus.* J Biomed Mater Res, 2003. **66A**(3): p. 605-14.
31. Tan, J.L., et al., *Cells lying on a bed of microneedles: an approach to isolate mechanical force.* Proc Natl Acad Sci U S A, 2003. **100**(4): p. 1484-9.
32. E. Ostuni, R.K., C.S. Chen, D.E. Ingber, G.M. Whitesides, *Patterning Mammalian cells Using Elastomeric Membranes.* Langmuir, 2000. **16**: p. 7811-7819.
33. Wójciak-Stothard B, M.Z., Korohoda W, Curtis A and Wilkinson C, *Activation of macrophage-like cells by multiple grooved substrata:Topographical control of cell behavior.* Cell Biology International, 1995. **19**: p. 485-490.
34. Folkman J, M.A., *Role of cell shape in growth control.* Nature, 1978. **273**: p. 345-349.

35. Chicurel ME , C.S., Ingber DE, *Celular control lies in the balance of forces.* Current Opinion in Cell Biology, 1998. **10**: p. 232-239.
36. Weber, N., et al., *Small changes in the polymer structure influence the adsorption behavior of fibrinogen on polymer surfaces: validation of a new rapid screening technique.* J Biomed Mater Res, 2004. **68A**(3): p. 496-503.
37. Schachter, D.M.a.J.K., *A synthetic polymer matrix for the delayed or pulsatile release of water-soluble peptides.* J. Control. Rel, 2002. **78**: p. 143-153.
38. Yu, C., S.S. Mielewczyk, K.J. Breslauer, and J. Kohn, *Tyrosine-PEG-derived poly(ether carbonate)s as new biomaterials. Part II: Study of inverse temperature transitions.* Biomaterials, 1999. **20**(3): p. 265-272.
39. Yu, C.a.J.K., *Tyrosine-PEG-derived poly(ether carbonate)s as new biomaterials. Part I: Synthesis and Evaluation.* Biomaterials, 1999. **20**(3): p. 253-264.
40. Tangpasuthadol, V., S.M. Pendharkar, and J. Kohn, *Hydrolytic degradation of tyrosine-derived polycarbonates, a class of new biomaterials. Part I: Study of model compounds.* Biomaterials, 2000. **21**: p. 2371-2378.
41. Jack R. Smith, A.S., Norbert Weber, Doyle Knight, Sascha Abramson, Joachim Kohn, *Integration of Combinatorial Synthesis, Rapid Screening, and Computational Modeling in Biomaterial Development.* Macromolecules Rapid Communication, 2004. **25**: p. 127-140.
42. J.C. Meredith, E.J.A., *LCST Phase Separation in Biodegradable Polymer Blends: poly(D,L-lactide) and poly(sigma-caprolactone).* Macromolecules Chemical Physics, 2000. **201**: p. 733-739.
43. Muhammed A. Al-Nasassrah, F.P., J. Michael Newton, *The effect of an increase in chain length on the mechanical properties of polyethylene glycols.* European Journal of Pharmaeutics and Biopharmaeutics, 1998. **46**: p. 31-38.
44. Faucheux, N.S., R.; Lutzow, K.; Werner, C.; Groth, T., *elf-assembled monolayers with different terminating groups as model substrates for cell adhesion studies.* Biomaterials, 2004. **25**(14): p. 2721-2730.
45. Emanuele Ostuni, B.A.G., Milan Mrksich, Carmichael S. Roberts, George M. Whitesides, *Adsorption of Proteins into Hydrophobic Sites on Mixed Self-Assembled Monolayers.* Langmuir, 2003. **19**: p. 1861-1872.
46. Alves, C.M.R., R. L.; Hunt, J. A., *Preliminary study on human protein adsorption and leukocyte adhesion to starch-based biomaterials.* Journal of Materials Science: Materials in Medicine, 2003. **14**(2): p. 157-165.
47. C.M. Nelson, S.R., J.L. Tan, C.S. Chen, *Degradation of Micropatterned Surfaces by Cell-dependent and Independent Processes.* Langmuir, 2003. **19**: p. 1493-1499.
48. Schauer, T.E., Claus D, *Organic polymer treatment - the way to modern pigments.* European Coatings Journal, 2003. **3**: p. 114-120.
49. J. Brandup, E.H.I., and E.A. Grulke; associate editors, A. Abe, D.R. Bloch., *Polymer Handbook.* 1999. **4**.
50. Tadakoro, H., *Structure and properties of crystalline polymers.* Polymer, 1984. **25**(2): p. 147-164.
51. Wenbing Hu, V.B.F.M., *Liquid-liquid demixing in binary polymer blend driven solely by the component-selective crystallizability.* Journal of Chemical Physics, 2003. **119**(20): p. 10953-10957.

52. M. Doytcheva, D.D., R. Stamenova, C. Tsvetanov, *UV-initiated crosslinking of Poly(ethylene oxide) with pentaerythritol Triacrylate in solid state.* Macromolecules Material Engineering, 2001. **286**(1): p. 30-33.
53. Haugland, R.P., *Handbook of Fluorescent Probes and Research Products.* 2002. **9th Edition**: p. 461.
54. Kovacs, A.J.G., A.; Straupe, C.*] Isothermal growth, thickening, and melting of poly(ethylene oxide) single crystals in the bulk.* Journal of Polymer Science, 1974. **50**: p. 283-325.
55. G Natta, I.W.B., G. Allegra, Acc. Naz. Lincei Rend, 1961. **31**: p. 350.
56. D.A. Winesett, S.S., J. Luning, H. Ade, *Tuning substrate surface energies for blends of polystyrene and poly(mthyl methacrylate).* Langmuir, 2003. **19**: p. 8526-8535.
57. Orban, J.M.C., Toby M.; Wagner, William R.; Jankowski, Ron., *Easily grafted polyurethanes with reactive main chain functional groups. Synthesis, characterization, and antithrombogenicity of poly(ethylene glycol)-grafted poly(urethanes).* Journal of Polymer Science, Part A: Polymer Chemistry, 1999. **37**(17): p. 3441-3448.
58. Henn, G.S., M.; Poths, H.; Ruecker, M.; Rabe, J. P., *Influence of order in thin smectic polymer films on the structure at the surface.* Physica B: Condensed Matter (Amsterdam), 1996. **221**(1-4): p. 174-184.
59. Doye, J.P.K., *Computer simulations of the mechanism of thickness selection in polymer crystals.* Polymer, 2000. **41**(25): p. 8857-8867.
60. Chattopadhyay, S.M., J. Carson, *Instability and dewetting of conducting-insulating polymer thin-film bilayers.* Macromolecular Rapid Communications, 2004. **25**(1): p. 275-279.
61. Patel, N., et al., *Printing patterns of biospecifically-adsorbed protein.* J Biomater Sci Polym Ed, 2000. **11**(3): p. 319-31.
62. A. El-Ghannam, L.S., J. Jones, *Laminin-5 coating enhances epithelial cell attachment, spreading, and hesmidesmosome assembly on Ti-6Al-4V implant material in vitro.* J. Biomed. Mater. Res., 1999. **41**: p. 30-40.
63. A. El-Ghannam, P.D., I. M. Shapiro, *effect of serum proteins on osteoblast adhesion to surface-modified bioactive glass and hydroxyapatite.* J. Orthopaed. Res., 1999. **17**: p. 340-345.
64. Aaron SGoldstein, P.A.D., *Effect of adsorbed fibronectin concentration on cell adhesion and deformation under shear on hydrophobic surfaces.* Journal of Biomedical Material Research, 2002. **59**(4): p. 665-675.
65. Bruce Albert, e.a., *Molecular Biology of the Cell.* 2002. **4th Edition**.